ats-17989 DRA

27207-6001-TU-00

File with N76-22214

RESEARCH INVESTIGATION OF THE PHYSICAL INTERACTIONS AND PHENOMENA ASSOCIATED WITH HYPERVELOCITY SUB-MICRON PARTICLES

FINAL REPORT

by

N. L. Roy

Prepared for
NATIONAL AERONAUTICS AND SPACE ADMINISTRATION
Headquarters
Contract No. NASW-2720

July 1975

TRW
SYSTEMS GROUP

ONE SPACE PARK • REDONDO BEACH, CALIFORNIA 90278

RESEARCH INVESTIGATION OF THE PHYSICAL INTERACTIONS AND PHENOMENA ASSOCIATED WITH HYPERVELOCITY SUB-MICRON PARTICLES

FINAL REPORT

July 1975

Prepared by: N. L. Roy
N. L. Roy
Member Professional Staff
Chemical Physics Group
Systems Group Research Staff

Approved by: J. F. Friichtenicht
J. F. Friichtenicht, Head
Chemical Physics Group
Systems Group Research Staff

TRW SYSTEMS GROUP
One Space Park, Redondo Beach, California 90278

ABSTRACT

Signals from impact ionization plasmas are studied as a means of performing microparticle composition analysis. Impact ionization signal response was measured in a time-of-flight (TOF) system for lanthanum hexaboride, carbonyl iron, and aluminum microparticle impacts on a tantalum target, primarily in the 1 - 8 km/s velocity range. Oscilloscope photographs of representative ion TOF signal response are given for each material studied. Graphs and histograms are presented of the total charge collected as well as the charge collected in each observed ion mass group. Data show that ion signals consist primarily of the lower ionization potential elements over the 1 - 8 km/s range. Aluminum from aluminum particle impacts was observed down to 2 km/s for most impacts. Data in the 20 km/s range show a marked improvement in the observed number of higher ionization potential elements. As the result of the greatly improved data yield above 10 km/s, it is recommended that missions above 10 km/s be considered for the use of an impact ionization TOF system to perform composition analysis. Preliminary data were acquired from impacts of carbonyl iron particles, differing in mass by two orders of magnitude, to determine mass dependent effects on total charge produced. Where $Q = K\, m^{\alpha} v^{\beta}$, α was found to be equal to 0.154. This value differs significantly from other results found over a smaller mass range which indicate α to be near unity.

TABLE OF CONTENTS

LIST OF ILLUSTRATIONS

LIST OF ILLUSTRATIONS (continued)

1.0 INTRODUCTION

In recent years an increasing degree of interest and discussion has been observed in regard to a possible flyby mission to probe the physical characteristics of one of the short period comets. In any such mission, a measurement of the physical parameters of the cometary dust environment would be of primary interest. Physical parameters to be measured are particle mass, number density, and chemical composition. The present study has examined the impact ionization phenomena as a means of measuring these parameters for a cometary encounter in a 1 - 8 km/s relative velocity range.

The impact ionization phenomena has been known for a number of years and is the result of vaporization and subsequent thermal ionization of a portion of both projectile and target materials from kinetic energy liberated during a high velocity impact. By use of appropriately structured electric fields, the ions produced may be extracted and subsequently analyzed in a time-of-flight mass analyzer. Such a system was used in the present study to examine the signal response obtainable for impacts of lanthanum hexaboride, carbonyl iron, and aluminum microparticles on a tantalum target, primarily in the 1 - 8 km/s impact velocity range.

In Section 2, a review of the basic principles of the impact ionization process is given in order to acquaint the reader with a model which describes the phenomena with sufficient clarity to permit in situ measurement of the relative abundance of materials in an impacting particle. This would be in addition to the simpler mass analysis and identification obtained from arrival time data in a time-of-flight system. The review in Section 2 details the way in which this may be accomplished by the addition of two or more control elements to the impact target surface in known relative abundance.

In Section 3, the impact ionization data acquired in the TRW Systems Group Microparticle Accelerator Facility are presented. A description of the microparticle accelerator and associated apparatus is given together with details of the experimental apparatus for measuring the impact signal response. The data are presented in the form of representative oscilloscope photographs of the signal response obtained over the

velocity range studied. The total impact charge signal was measured for each impact and also the quantity of charge contained in each observed ion group. These data are presented in the form of graphs and histograms for each of the particle materials studied.

Section 4 is a summary and discussion of the study with recommendations in regard to a possible cometary flyby mission.

2.0 REVIEW OF BASIC PRINCIPLES

The material to be presented later in this report involves the laboratory investigation of the impact ionization effect at low impact velocities. The primary objective of the program was to determine the capability of an instrument using impact ionization to measure chemical composition of cometary debris at low fly by speeds. A basic review of the impact ionization effect and the techniques employed in an impact ionization time-of-flight instrument will be given in this section prior to a discussion of the laboratory results of this program. The material presented is taken in part from a previous report by this organization under NAS 9-9309.[1]

2.1 The Impact Ionization Model

It was first shown experimentally by Friichtenicht and Slattery[2] that free electrical charge, both positive and negative, is produced at the point of impact of a high velocity particle on a solid surface. More recent experiments have shown that the positive charge consists of ions of both the impacting particle and target materials and that the negative charge carriers are electrons. The experimental results obtained and presented in Reference 1 above has demonstrated this effect in considerable detail at high impact velocities.

Based upon a detailed analysis of these experiments, a theoretical model to describe the impact ionization effect has been developed.[3,4] In this model, it is assumed that a small, high-density plasma in thermal equilibrium is formed in the immediate vicinity of the impact site. The plasma expands to a collisionless state in a time short compared to the characteristic recombination time of the ions and electrons. Thus, shortly after impact, free ions and electrons are expanding radially outward from the impact site with a velocity distribution characteristic of the initial plasma temperature. In the presence of a modest electric field, the ions and electrons can be separated and subsequently analyzed by time-of-flight techniques.

2.1.1 Supporting Evidence for the Plasma Model

It should be stated that a detailed knowledge of cratering and energy conversion mechanisms is not required in order to apply the impact plasma concept to the determination of cosmic dust composition. Nevertheless, it is useful to review some of the known details of the impact process in order to show that the proposed model is compatible with them.

Consider the case of a small particle impacting a metallic surface. It is well known that at low impact velocities much of the kinetic energy is expended in elastic and plastic deformation of the target and in the ejection of relatively massive fragments of the target material. At high impact velocities, however, the energy release is localized to a relatively smaller volume because the particle penetrates the material with a velocity large compared to the shock wave velocity in the medium. This interface velocity v_I may be taken as one-half the initial particle velocity. To first order, the time required to form the crater is given by the ratio of the crater depth P to the average interface velocity.

Experiments show that a more-or-less hemispherical crater is formed in the target with a depth that is, at most, several times the particle diameter d. By selecting high-density, high-strength target materials (e.g., tantalum, tungsten) the ratio P/d can be limited to a value of three or four, even for very high impact velocities. This being the case, the kinetic energy per atom of the impacting particle is shared with an average of 15 to 30 target atoms. Now at an impact velocity of 20 km/s, an iron atom has a kinetic energy of about 120 eV. If this energy is shared with all of the ejected target atoms, the average energy per atom is between 4 and 8 eV. An average energy of this magnitude is sufficient to completely vaporize the particle material and the ejected target material, and also to ionize a substantial fraction of the atoms in the ejected vapor cloud.

For the plasma model to be valid, it is necessary that the conversion of the kinetic energy of the impacting particle to internal energy of the expanding, partially-ionized vapor cloud occur in a time short compared to competing methods of energy absorption, such as plastic deformation, heat conduction, etc. To show that this is in fact the case, we note that an order-of-magnitude estimate of the time interval Δt during which energy is deposited in the target can be obtained by writing $P \approx v_I \Delta t$. Consider an impact of a 10 micron diameter iron particle with velocity v = 20 km/s (or 2×10^6 cm/s) on a reasonably hard metal target. If the crater produced has a P/d $\approx$ 4, then $P \approx 4 \times 10^{-3}$ cm and $v_I \approx v/2 = 10^6$ cm/s, and so $\Delta t \approx 4 \times 10^{-9}$ sec. It would appear unreasonable that any of the likely competing energy absorption mechanisms could be effective in this small a time interval.

On the other hand, the time Δt is also short compared to the time required for appreciable expansion of the vapor cloud, since a reasonable expansion velocity for such a plasma might be $\sim 2 \times 10^5$ cm/s. During the time Δt, the plasma density must be very close that of the solid material, in which case the mean time between atomic collisions is $\sim 10^{-13} - 10^{-14}$ seconds. Because the time scale for interatomic collisional energy exchange is so short compared to that required for expansion of the plasma, it seems very reasonable to conceive of the plasma being in thermal equilibrium.

If the plasma expansion velocity is 2×10^5 cm/s, the plasma density is reduced by a factor of 10^6 per microsecond, with the collision frequency being reduced correspondingly. This time scale is again short compared to that acquired for competing energy absorption mechanisms.

Bjork[5] has shown theoretically that the crater volume becomes proportional to the momentum of the impacting particle at high velocities. This implies that the energy density of the ejected material (i.e., average energy per atom) increases linearly with the impact velocity. One might expect that this would result in an increased plasma temperature at higher impact velocities, and there is ample experimental evidence that this is generally true. However, recent experiments have

shown that the partition of energy is such that a fairly wide range of apparent plasma temperatures occurs at a given impact velocity. Both topographical and physical characteristics of the surface at the impact site probably contribute to this variation.

2.1.2 Consequences of the Model

For a plasma in thermal equilibrium containing several species of atoms, the degree of ionization of each species and the plasma temperature are related according to Saha's equation:[6]

$$\frac{n_e n_i^s}{n_n^s} = 2G(2.414) \times 10^{15}\, T^{3/2} \exp\,(-E_I^s/kT) \qquad (1)$$

where

n_e = total number of electrons per cubic centimeter,

n_i^s = number of ions of species s per cubic centimeter,

n_n^s = number of neutral atoms of species s per cubic centimeter,

$G = P_i^{int}/P_n^{int}$, where P_i^{int}, P_n^{int} are the internal partition functions of the ions and atoms, respectively,

T = plasma temperature in °K,

E_I^s = ionization energy of species s,

k = Boltzmann's constant.

The Saha equation shows that the fractional ionization of a given species of atom depends on the ratio of the ionization energy of that species to the mean thermal energy of the plasma. For reasonably low plasma temperatures, only a small fraction of the atoms are ionized (except for those with very low ionization potentials). Thus, in order to use the impact ionization effect to reliably determine the relative abundance of the elements in cosmic dust and meteoroids, a measure of the plasma temperature must be obtained.

In addition, it would at first appear that the number density of ions, electrons, and atoms must be specified. However, from the argument given above, the plasma expands to a collisionless state in a time short compared to the ion-electron recombination time. As a consequence, the total number of ions is constant at any time during the expansion process. Since all of the ions regardless of species are extracted from the same volume, a direct measurement of n_e, n_n^s, and n_i^s is not required to determine the relative abundance of the different kinds of atoms. If N_e, N_n^s, and N_i^s are, respectively, the total numbers of electrons, atoms, and ions in the plasma, and if V is the volume of the plasma at any time prior to its expansion to a collisionless state, then $n_e = N_e/V$, $n_n^s = N_n^s/V$, and $n_i^s = N_i^s/V$. Clearly, $n_e n_i^s/n_n^s$ can be replaced in Equation (1) by $N_e N_i^s/N_n^s V$*.

A viable experiment must be configured to provide a direct measurement of both N_i^s for each s and also N_e. (If all N_i^s are measured, N_e can be obtained from $N_e = \sum_s N_i^s$, since the total number of ions and electrons are equal; however, an independent measurement of N_e is readily obtained and serves as a useful check of the data.) The quantity of principal interest, however, is N_n^s and the plasma temperature must be specified in order to extract this quantity from the experimental data. There appear to be two methods of experimentally determining the plasma temperature. One method is the measurement of the width of the ion peaks. The second method consists of measuring the ratio of the numbers of two "control" ion species formed from atoms that are present in the plasma in a known relative concentration.

The first method depends upon the fact that the energies of ions in an equilibrium plasma are given by a Boltzmann distribution. As the temperature is increased, the mean ion energy increases and the spread in energies becomes larger. Thus, a measurement of the width of the ion energy distribution of any species of ion would provide a measure of

*V need not be determined, since it drops out when ratios are taken, as will be shown shortly (Eq. 2, following page).

the plasma temperature. However, this approach would place extremely stringent, if not impossible, bandwidth requirements on the electronic analyzing and recording system.

The second method appears to be the more promising approach. There are at least two ways in which the two control ion species may be introduced into the plasma. One is through the use of thin film layers of the desired elements on the target surface. The second is by using a target with the two elements "mixed" homogeneously throughout. The latter could conceivably be accomplished with an alloy type material, but a better approach appears to be the use of a material in which the two elements exist in molecular form and therefore in a known stoichiometric ratio.

For purposes of discussion, consider the case where the two elements will be introduced into the plasma by the vapor deposition of thin films of the two elements onto the target surface. The combined thickness of the two films must be small compared to the expected crater depth. Under these conditions, atoms from the two films become intimately mixed within the plasma with atoms from the impacting particle. (Atoms from the target bulk material are also included within the plasma; however, they will not be used in the detailed analysis of the data, and the only requirement placed on the bulk target material is that it confine energy release to a small volume.) Given the film thicknesses, the number of both kinds of atoms per unit area of the impact surface is specified. For crater diameters large compared to the film thickness, the relative number of the two different kinds of atoms introduced into the plasma volume is known independently of the crater volume. Now, the Saha equation holds for the ion-to-neutral ratio of both kinds of atoms. Denoting the two types of control atoms by superscripts (1) and (2) and dividing the Saha equation for one species by the Saha equation for the other yields

$$\frac{N_i^{(1)} N_n^{(2)}}{N_i^{(2)} N_n^{(1)}} = k_1 \frac{\exp\left[-E_I^{(1)}/kT\right]}{\exp\left[-E_I^{(2)}/kT\right]} , \qquad (2)$$

where k_1 is a known constant. For $N_n^s > N_i^s$, which is almost always the case, the ratio $N_n^{(1)}/N_n^{(2)} = k_2$ is approximately the relative concentration of the two kinds of atoms in the thin films, which is known. Now assume that the elements have been chosen such that $E_I^{(2)} \neq E_I^{(1)}$. We can write $E_1^{(1)} = E_1^{(2)} + \Delta E_I$. Substitution into (2) yields

$$\frac{N_i^{(1)}}{N_i^{(2)}} = k_1 k_2 \frac{1}{\exp\left(\Delta E_I/kT\right)} , \qquad (3)$$

from which

$$T = \frac{\Delta E_I}{k \ln\left\{k_1 k_2 \left(\frac{N_i^{(2)}}{N_i^{(1)}}\right)\right\}} . \qquad (4)$$

With the temperature thus specified, the procedure can be reversed to yield the relative abundance of all of the elements contained in the impacting cosmic dust particle.

The choice of appropriate materials to be used for the thin films depends upon several factors:

(1) The ionization potentials of the two elements must differ by two or three electron volts in order to obtain a substantial change in the ratio $N_i^{(1)}/N_i^{(2)}$ as the plasma temperature varies.

(2) The ionization potentials must be low enough to ensure a sufficient degree of ionization to obtain detectable signals.

(3) The mass of the atoms should lie outside of the mass range of elements expected from the cosmic dust particles.

(4) The films must be stable when exposed to the space environment and the materials must be compatible with uniform vapor deposition.

2.2 Experiment Implementation

For flight applications, time-of-flight (TOF) ion mass analysis is the most straightforward technique for acquisition of the desired data. This approach has been utilized for laboratory experiments as well. A sketch of a simplified laboratory TOF analyzer is shown in Figure 2-1. In this instrument, the impact surface is maintained at a positive potential V_A with respect to its surroundings. A grounded accelerator grid is placed parallel to the impact surface at a separation distance L_1, and an ion collector is located a distance L_2 from the grid.

Upon impacting the target surface, a high velocity particle produces an impact plasma which immediately begins to expand. As the plasma approaches the collisionless state, the ions and electrons separate due to the electric field between the grid and the impact plate. The electrons are returned to the impact plate, while the ions are accelerated toward the grid. When they reach the grid plane the ions have a velocity given by

$$v = \left(\frac{2e}{\mu} V_A\right)^{1/2} \tag{5}$$

where e/μ is the charge-to-mass ratio of the ions. The region between the grid and the ion collector is field-free, and the ions drift to the ion collector at constant velocity. Neglecting any initial velocity of the ions and assuming that the plasma is small compared to the grid-to-target separation, the time τ required for the ions to traverse the distance from the impact plate to the collector is

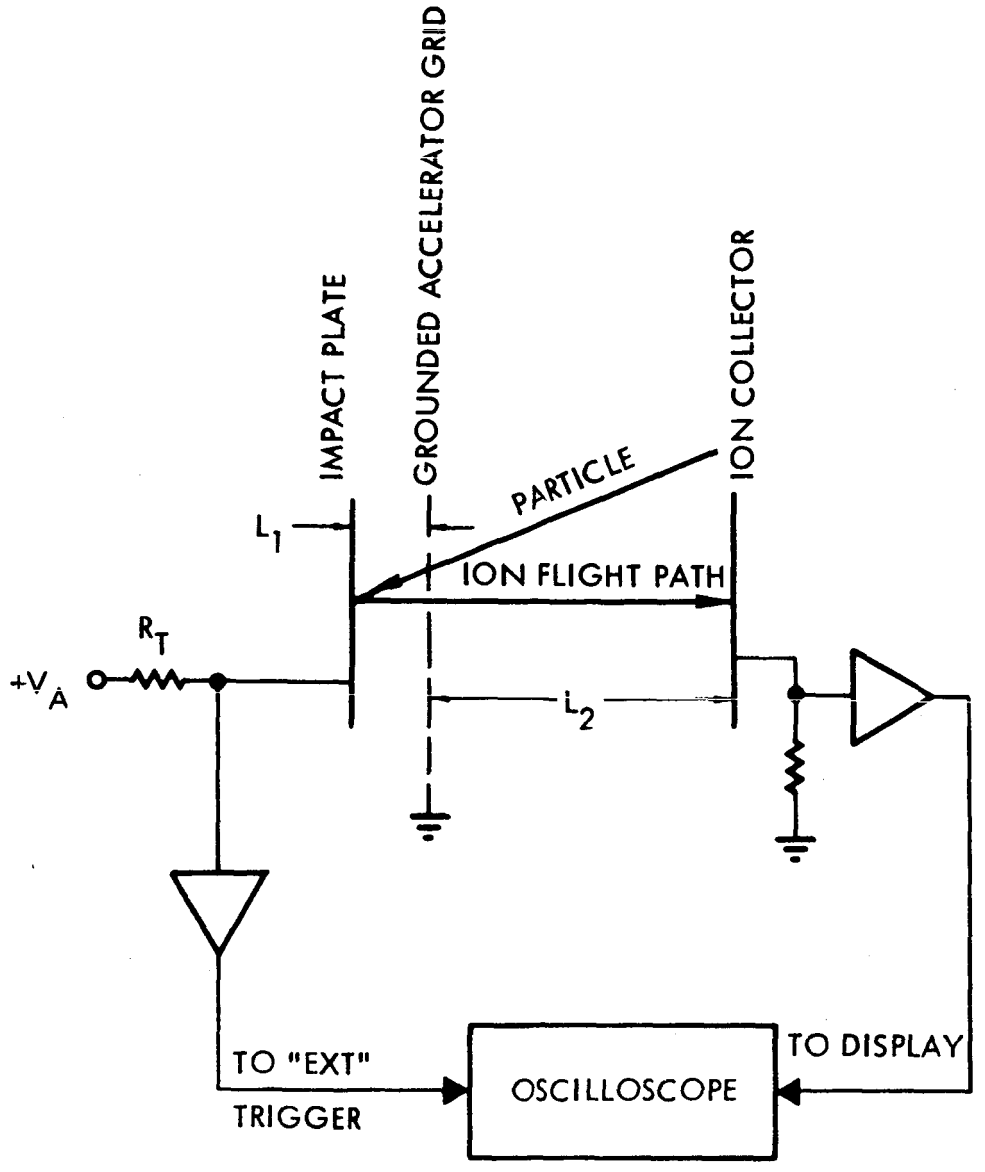

Figure 2-1. Sketch of a Simplified Time of Flight Analyzer. Particles pass through accelerator grid and strike impact plate, forming a microplasma at the impact site containing ions of the particle (and impact plate) material. Positive extraction potential applied to plate accelerates ions from plasma toward grid and returns electrons to plate. Departing ions produce target signal which starts scope sweep. Ions, passing through accelerator grid drift in field-free region to ion collector, arriving there in a time dependent on their charge-to-mass ratio. Positive ion charge at collector is amplified and displayed on scope.

$$\tau = \left(\frac{\mu}{2eV_A} \right)^{1/2} (2L_1 + L_2) \quad . \tag{6}$$

Thus, a measurement of the transit-time of an ion group uniquely defines the charge-to-mass ratio of ions in the group. Assuming singly ionized atoms (which is much more likely that multiply-ionized atoms because of the relatively low plasma temperatures involved), the ion TOF measurement defines the atomic mass and hence identifies the element. It should be noted that the presence of the two control elements used to determine the plasma temperature in the flight experiment also provides a calibration of the ion TOF range, since these two ion groups always appear. The number of ions of each element in the impacting particle (plus those from the vapor-deposited films and the target material) can be determined by integration of the ion current arriving at the collector.

The most convenient and satisfactory method of acquiring the desired data in the laboratory is the photographic recording of an oscilloscope display. Figure 2-1 also shows how such a display is produced. The collection of electrons at the impact plate essentially coincides with the time of impact of the particle on the surface, and thus the electron pulse at the target provides a "start" pulse for the ion TOF measurement. The electron current flow through R_T develops a voltage pulse to start the sweep of the recording oscilloscope. The amplified signal from the ion collector is displayed on the oscilloscope trace; there the ion collector amplifier can be either current- or charge-sensitive. In the current-sensitive mode, one observes a series of peaks of varying amplitudes and time locations corresponding to ions of different elements. In the charge-sensitive (integrated) mode, the signal increases in steps to its maximum value and then decays with some long time constant. The leading edge of each of the steps specifies the arrival time of an ion group and the amplitude of each step gives the total charge associated with that particular ion group.

Equation (6) shows that the total ion transit time τ for a given e/μ is proportional to $(2L_1 + L_2)/V_A^{1/2}$, which can be rewritten as $L_T/V_A^{1/2}$ where $L_T = 2L_1 + L_2$. (It is assumed that $L_2 >> L_1$.) From this it appears that τ can be adjusted to any convenient value by adjusting the accelerating potential and the total flight path length. However, there exists a practical lower limit to the accelerating potential due to the fact that the ions possess finite thermal energies. This affects both the radial expansion of the accelerated ions and the ion transit time. Although the mean thermal energy may correspond to no more than a few electron volts, the energy distribution curve is sufficiently wide so that some ions with energies of a few tens of electron volts are often observed.

In order to obtain some feeling for suitable values of L_T and V_A, let us assume that the thermal ion energies range from zero to E_o and that the corresponding velocity vectors are randomly oriented. The initial energy can be expressed in terms of an equivalent accelerating potential V_o which would impart to the ion a final energy of E_o. First examine the radial expansion of the accelerated ions. The worst case occurs when the initial velocity vector is perpendicular to the direction of the applied electric field. This yields a normal velocity component $v_n = (2e\ V_o/\mu)^{1/2}$. The velocity component due to the applied electric field is parallel to the field and is given by Equation (5). The angle between the resultant velocity vector and the electric field vector is given by

$$\theta = \tan^{-1}\left(\frac{v_n}{v}\right) = \tan^{-1}\left(\frac{V_o}{V_A}\right)^{1/2} \qquad (7)$$

In order to ensure complete ion collection, the ion collector radius must satisfy

$$R_C \geq L_T\left(\frac{V_o}{V_A}\right)^{1/2} \qquad (8)$$

Thus, for $V_o = 30$ volts, $V_A = 3000$ volts, and $L_T = 1$ meter, R_C must be at least 10 centimeters.

The range of initial velocity components parallel to the electric field lines causes a broadening of each ion peak and affects the ultimate mass resolution of the TOF mass spectrometer. Let us arbitrarily assume that we would like to just resolve atomic mass number 60 (nickel) from mass number 56 (iron). The worst case occurs for a nickel ion with maximum initial energy and an iron ion with zero initial energy. Requiring that the transit time of these two ions be equal ensures complete resolution of the iron and nickel peaks, because less energetic nickel ions require a longer transit time. This requirement gives:

$$\frac{L_T}{2V_A}\left(\frac{e}{\mu}\right)^{-1/2}_{Fe} = \frac{L_T}{\sqrt{2(V_A + V_o)}}\left(\frac{e}{\mu}\right)^{-1/2}_{Ni} \qquad (9)$$

from which it follows that

$$V_A = V_o\left[\frac{(\mu)_{Fe}}{(\mu)_{Ni} - (\mu)_{Fe}}\right] = 14\ V_o \quad .$$

Assuming as before that V_o = 30 volts, V_A need be only 420 volts which is less than the value required to limit excessive radial expansion of the accelerated ions. Thus, in practice, fixing V_A to minimize the expansion problem will more than satisfy the mass resolution considerations arising from the nonzero initial thermal energies.

3.0 LABORATORY INVESTIGATION OF IMPACT IONIZATION

3.1 Program Objectives

A variety of previous impact experiments have been conducted which show the unique capability of an impact ionization time-of-flight instrument to perform in situ chemical composition analysis on an impacting cosmic dust particle. To a large extent the previous work has been limited to velocities above 10 km/sec where the major interest has been in the analysis of the micrometeoroid environment. Recent consideration of possible cometary rendezvous missions at flyby speeds below 10 km/sec has prompted the present study.

The specific objective of the present program was to perform analyses of impact ionization plasmas in the 1 to 8 km/sec range. This was accomplished in a laboratory time-of-flight arrangement which will be described in the following subsections. Specific interest in the analyses would be in determining the usefulness of the technique in microparticle detection and chemical characterization if used in a low velocity cometary flyby application.

3.2 The Experimental Facility

The impact ionization experiments conducted under the present program were accomplished at TRW using the TRW Microparticle Facility. A general descrition of the systems and the experimental arrangement used will be given to provide a better understanding as to the nature of the experiments performed. A knowledge of the experimental configuration is essential for ease of interpretation of the data presented.

3.2.1 The Microparticle Accelerator and Associated Apparatus

The block diagram in Figure 3-1 shows the microparticle accelerator and the various subsystems necssary for the impact ionization tests. To the left in the Figure may be seen the microparticle accelerator in block form. To the right is indicated the time-of-flight (TOF) chamber in which the experiments were conducted. The details of the TOF chamber will be described later. The region between the accelerator and the TOF chamber contains the various microparticle beam detection apparatus and particle sorting equipment.

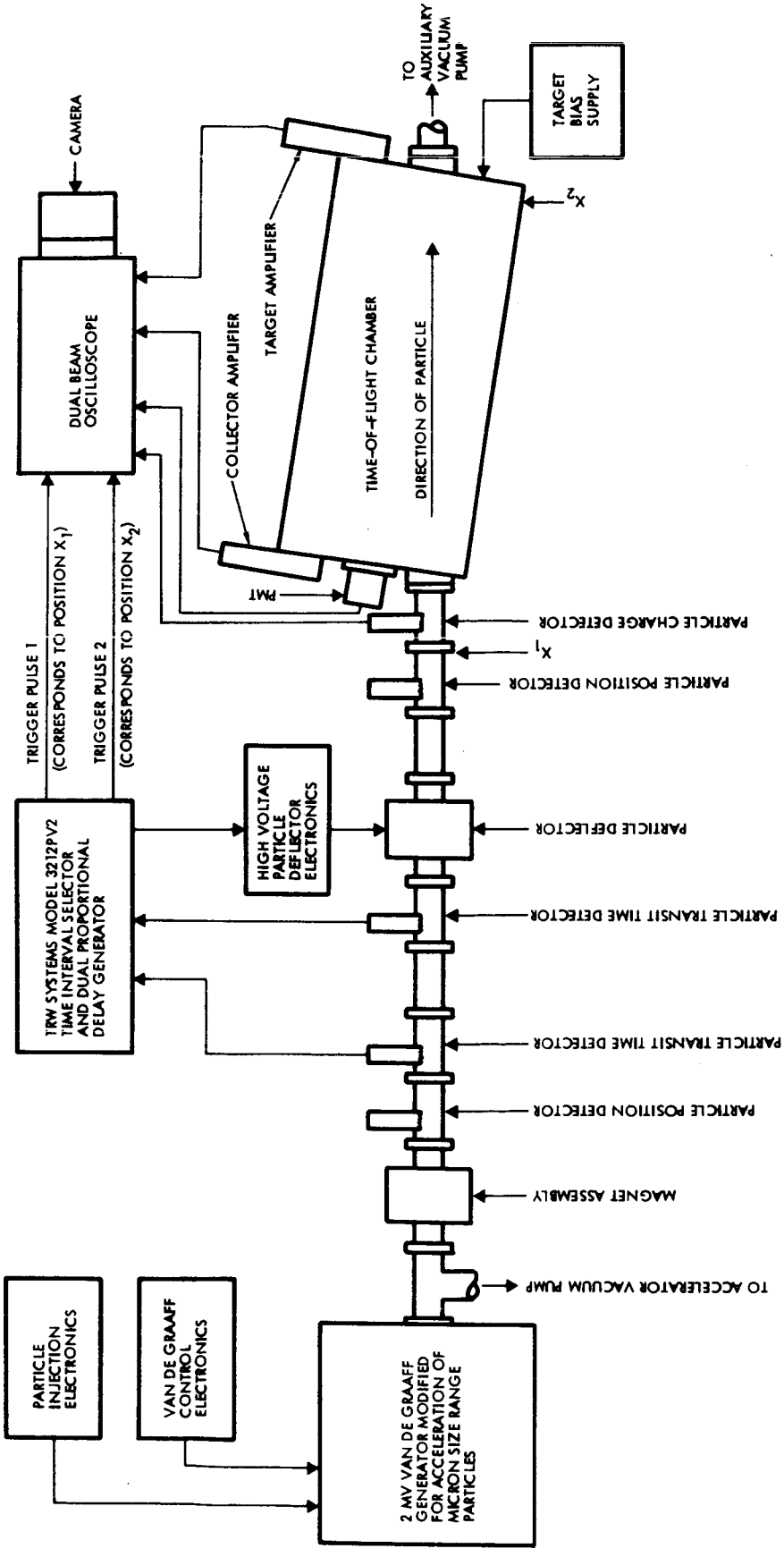

Figure 3-1. Block Diagram of TRW Systems Group Micrometeoroid Simulation and Test Facility, showing experimental setup for impact ionization studies.

The particle accelerator is a two million volt Van de Graaff generator in which the high voltage terminal has been modified to accept microparticle charging and injection equipment.[7] The modified accelerator is capable of charging and accelerating a variety of micron size range materials to high velocities. The final particle exit velocity obtained is dependent upon the size of the particular particle, the material used, and the accelerating potential. Particle velocities range down to well below one kilometer per second for all materials. The upper velocity limit is, for practical purposes, dependent upon the sensitivity of the electronics used for particle detection. For carbonyl iron particles the maximum detectable velocity is above 50 km/sec; for lower density materials the maximum detectable velocity may exceed 100 km/sec. The particle beam from the accelerator is electronically gateable and may be set to produce a single output particle or a flux of several hundred particles per second.

Particles exiting from the accelerator first pass through a magnet assembly where ions, which may have been produced by the charging process, are removed. A particle position detector[8] then provides a means for locating the particle "beam" axis in order to align the system. The particles next pass through two detectors spaced apart a carefully-measured distance, from which the transit time over this distance may be measured. the time separation of the two detector signals is analyzed by a TRW Systems Model 3212PV2 Time Interval Selector and Dual Proportional Delay Generator.[9] This unit has two principal functions: First, it provides an output pulse to a particle deflector when the measured transit time falls within the bounds of some predetermined time interval. Normally, with no signal applied to the input of the particle deflector high voltage electronics, all particles are deflected by a bias voltage on a pair of deflector plates and are not allowed to continue downstream toward the experimental area. A signal from the Time Interval Selector removes the bias voltage for a time just sufficient to allow the selected particle to pass. The selected particle continues downstream through a sensitive charge detector[10] and into the experimental chamber. Second, the Time Interval Selector contains proportional delay generators which produce two trigger pulses at adjustable multiples of the actual measured transit

time. By proper adjustment of the multiplication factors, these pulses can be made to appear when the selected particle is at two arbitrarily selected points downstream, independent of particle velocity. The pulses are used to start oscilloscope sweeps; the first is generally set to occur just before the particle enters the particle charge detector (position X_1, Figure 3-1), and the second is set to occur just prior to the particle interacting with the experiment. In this case, the second trigger occurs when the particle is nominally at the position labeled X_2 on Figure 3-1, which is just prior to impact on the target.

The Time Interval Selector together with the particle deflector and associated electronics comprise a particle sorting system which effectively monitors the exit beam from the accelerator and removes all particles with velocities which lie outside the desired range. Although not shown in the Figure, the particle selection system also contains window discriminators to permit the control of particle charge. Control of both particle charge and velocity in effect controls the particle mass for a given accelerator potential and particle material.

Particles which have the desired parameters are permitted to pass through the particle charge detector and into the time-of-flight chamber where they collide with the target plate at the downstream end of the chamber. Electronics are available for monitoring the charge which leaves the target and also for that arriving at the upstream end of the chamber. Output signals from the particle detector, target electronics, and collector assemblies are displayed on a dual beam oscilloscope. The oscilloscope display is normally recorded photographically for later measurement and analysis of the signals produced by each individual particle impact. A more detailed description of the TOF chamber is given in a subsequent section.

3.2.2 Microparticle Linear Accelerator

Some of the data acquired under this program utilized the Microparticle Linear Accelerator[11] available at the TRW Microparticle Facility. The experimental arrangement using the linear accelerator is not shown separately in the figure. To utilize the linear accelerator in impact experiments, the system shown in Figure 3-1 is broken at the point marked

X_1 and the particle charge detector and time-of-flight chamber is positioned at the output end of the oscillator. Velocity selection equipment and oscilloscope sweep triggers are available as a part of the linear accelerator system. The overall system works in a manner similar to that described above with the exception that the linear accelerator operates at a reduced rate of about one particle per minute maximum. The net accelerating potential used for this program was approximately six million volts. At this accelerating potential and at the same velocity, the particle mass would normally be about 60 times the particle mass available from the Van de Graaff accelerator at 1.5 million volts. Some of the work performed on this program utilized the linear accelerator to obtain larger mass particles which permitted a check on possible mass effects in the impact ionization process.

3.2.2.1 Experimental Configuration

Figure 3-2 is a more detailed block diagram of the experimental arrangement used for the collection of impact ionization data using the microparticle accelerator. In this Figure the TOF chamber is shown in bold outline connected to the microparticle accelerator. The target assembly and collector assembly may be seen in schematic form at their respective locations.

The enclosure for the target and collector assemblies is a cylindrical vacuum tank about 46 centimeters in diameter and 125 centimeters in length. The target assembly consists of a cylindrical metal enclosure which acts as a shield to prevent stray electric fields from entering the TOF range. The side of the enclosure nearest the center of the chamber is gridded to permit particles to enter and ions to leave from the target. The impact target plate is mounted approximately one centimeter from the enclosure grid and is biased at +3000 volts. The resulting electric field of 3000 volts per centimeter extracts ions from the vicinity of a particle impact and accelerates them in a direction parallel to the axis of the tank. Hermetically sealed cable bulkhead connectors provide means for introducing the target bais voltage and extracting the impact signal from the target.

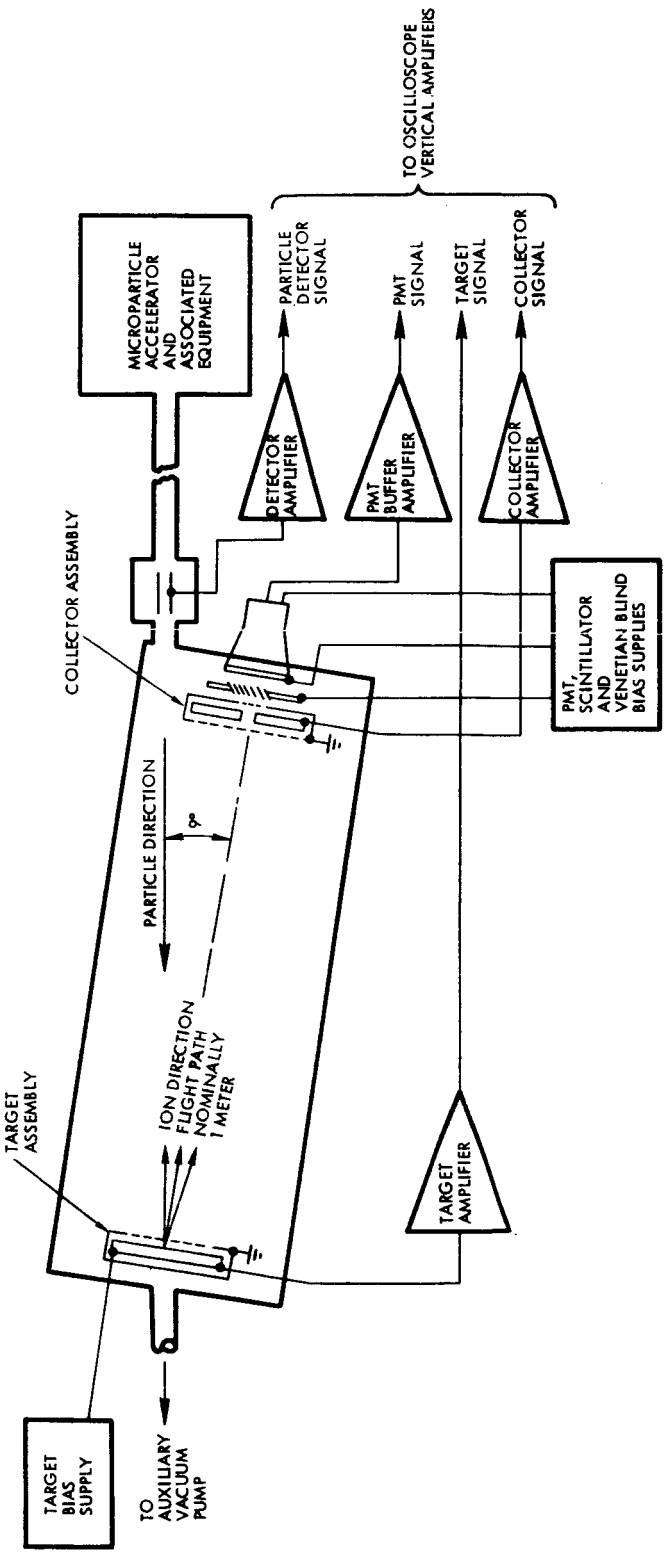

Figure 3-2. Detailed Block Diagram of Experimental Configuration, with schematic representation of target and collector assemblies inside time-of-flight chamber.

The ion collector assembly is positioned on the axis of the tank approximately one meter from the target assembly. The ion collector assembly uses two quite different techniques for detection of charge arriving from the target. The first method uses a 20 centimeter diameter disc mounted within a cylindrical metal enclosure for collection of arriving ions. The side of the enclosure nearest the center of the tank is formed from a high transmission grid ($\approx$95%) to permit ions to pass through to the collector plate. A bias voltage of +80 volts was normally applied to the collector plate to retain any secondary electrons which may be produced by ion impact. The signal generated on the collector plate is brought outside the tank, again through a hermetically sealed cable connector, to the collector amplifier. The amplifier may be either charge sensitive or current sensitive. In the charge sensitive mode, the arriving current is integrated and the output signal will be staircase-like in appearance with each step corresponding to the charge collected in a particular mass group. If the output is current sensitive, then the signal will appear as a series of spikes of varying amplitudes which correspond to the time history of arriving ion current.

The second means of ion detection is a much more sensitive one and will in effect permit single ions to be counted if this is desired. The sensitive ion detector assembly may be seen to the right of the collector assmebly in Figure 3-2 and is shown in greater detail in Figure 3-3. The ion detector shown employs techniques which: (1) converts the ion to be detected to one or more secondary electrons; (2) adds energy to the secondary electrons; (3) converts a portion of the electron energy into photons by impacting an appropriate scintillator material; and (4) detects the photons generated with a low noise photomultiplier (PMT).

An operational description of the unit follows: Some of the ions arriving at the collector plate are permitted to pass through a 2.5 centimeter diameter hole in the center. After emerging from the gridded opening at the back of the collector plate assembly, the positive 3000 volt ions are accelerated through an additional 9000 volts and finally strike a venetion blind fixture where secondary electrons may be produced. When emitted from the venetian blind surface, the electrons are in an electric field which directs and accelerates them toward a five

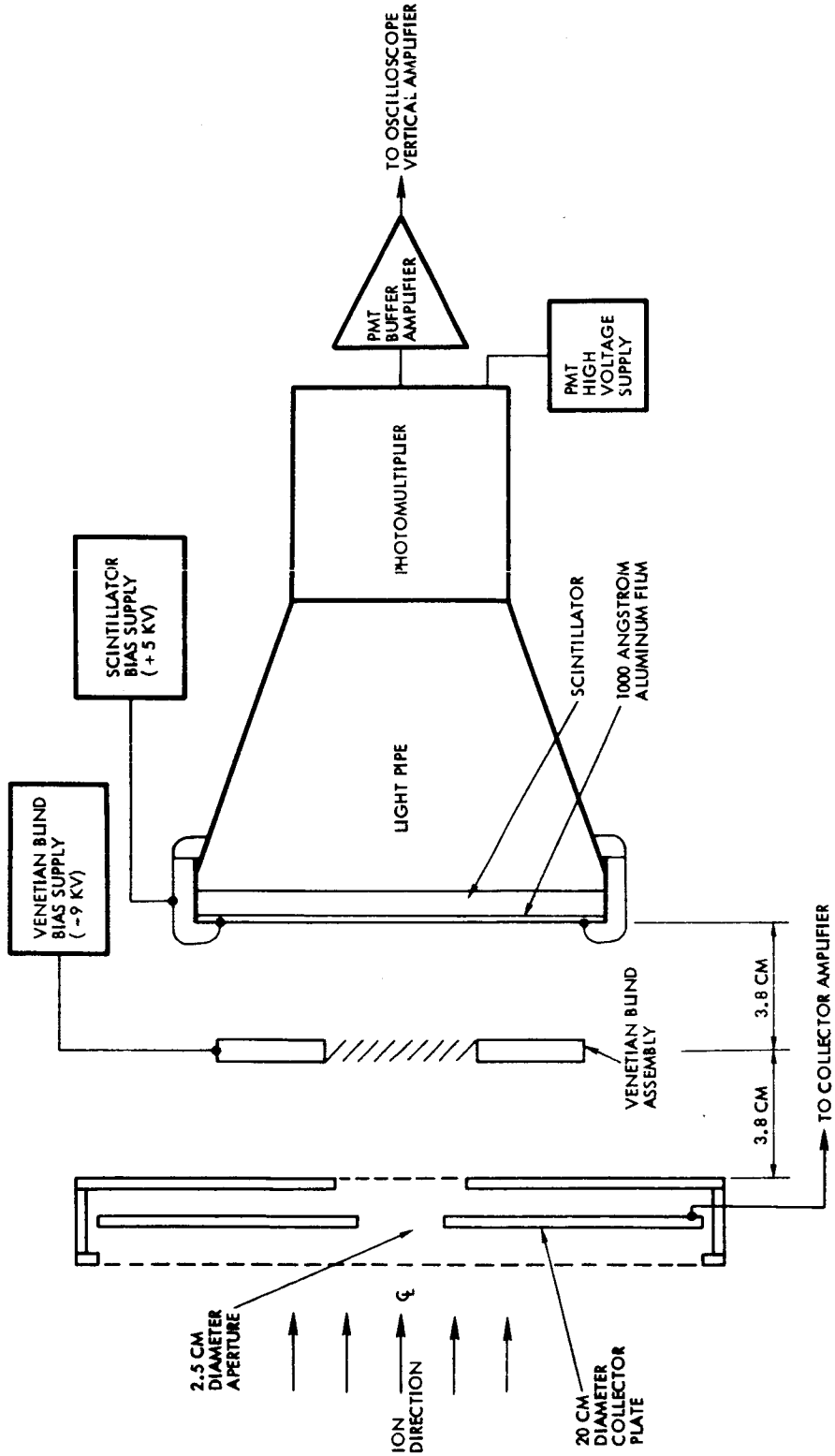

Figure 3-3. Diagram of Collector Plate and Sensitive Ion Detector Assembly.

inch diameter cylindrical scintillator. The surface of the scintillator is covered with a 1000 Å vacuum deposited aluminum film which serves as an anode for the electrons and also prevents light from entering or leaving from the scintillator. The thin aluminum film was normally biased to +5000 volts thereby causing the electrons to impact the surface with an energy of 14,000 electron-volts. The range of the electron is sufficient to permit them to pass through the aluminum film and to generate photons within the scintillator. The photons produced are conducted through a light pipe to the photocathode of a PMT as shown. The resultant PMT anode signal is buffered with an amplifier and presented to one of the vertical amplifiers of the oscilloscope for display. Again, as with the collector plate, the output signal may be a current waveform proportional to the incident ion current for a particular mass species or the output current may be integrated on a capacitor thereby permitting relative charge measurements to be made.

Operationally, the sequence of events begins when a particle exiting from the accelerator is found, by the Time Interval Selector, to have a transit time within the preselected transit time boundaries. This event causes the bias voltage on the particle deflector to be removed thereby allowing the selected particle to enter the experimental area. Just prior to arrival of the particle at the particle detector, shown schematically in Figure 3-2, the Proportional Delay Generator produces an output pulse which initiates an oscilloscope sweep thereby displaying the signal amplitude and transit time information produced by the particle as it passes through the detector. The displayed detector signal permits the particle velocity, mass, and radius to be calculated for each particle. Just before the particle reaches the target plate a second signal from the Proportional Delay Generator starts the second beam of the dual beam oscilloscope. This beam is used to display the target signal and the ion charge and transit time information from the collector or PMT.

3.3 Discussion of Laboratory Impact Ionization Data

The primary objective of the program was to study the ionization characteristics at low impact velocities and to determine the feasibility

of applying the technique to perform particle composition analysis on a low velocity cometary intercept mission. The velocity range of interest for the purposes of this study was 1-8 km/sec.

The three particle materials selected for use in the study were lanthanum hexaboride, iron, and aluminum. Lanthanum hexaboride was selected as the molecular compound material principally because it generally provides trouble-free operation in the microparticle charging apparatus. Iron and aluminum were selected as representative of the atomic materials which might be expected to be present in meteoroid or cometary particles. In terms of ionization potential of the atomic constituents, these materials also provide a reasonably good cross-section of the metallic elements which may be present in cosmic particles. The ionization potential of the selected elements are; boron, 8.30 eV; lanthanum, 5.61 eV; iron, 7.87 eV; and aluminum, 5.98 eV. Ionization potential is one of the most important parameters to consider when thermal ionization is providing the source of ions, as is evident from the discussion in Section 2. A more detailed discussion of the relative importance of ionization potentials will be undertaken in a later subsection.

The target plate selected for use in the experiments was a 0.25 millimeter thick tantalum sheet. No special precautions were taken to obtain a pure tantalum specimen since it was assumed that any impurities in the material would simply add more identifiable atomic elements. However, any surface layers of contaminants which might approach a fraction of a micron in thickness could possibly cause a change in the ionization produced over that from a clean tantalum surface. To avoid this possible complication the target material was cut to the appropriate target dimensions and thoroughly cleaned using standard laboratory degreasing techniques. The target sample was then placed in hard vacuum ($<10^{-5}$ Torr) and electrically heated by passing a high current through the material. A 2000°C temperature was attained, as determined by an optical pyrometer, and held for 30 minutes. The target was then transferred, untouched, to the target holder in the TOF chamber. It was felt that this treatment should remove any volatile contaminants which might still be on the surface after the standard cleaning procedures.

3.3.1 Lanthanum Hexaboride Particle Impacts

Figure 3-4 shows four oscilloscope photographs that are representative of the type of ionization signals obtained for the lanthanum hexaboride (LaB_6) impacts on a tantalum target. In each photograph the upper trace is the sum of the particle charge detector signal, the target signal, and the collector signal obtained by integrating the arriving ion current. The lower trace in Figure 3-4a, b, c is the sum of the target signal and the integrated collector signal while that in Figure 3-4d is the sum of the target signal and the collector (PMT) current waveform.

The particle charge is found from the amplitude of the rectangular pulse on the upper trace which is produced as the particle traverses a 10.0 cm long particle charge detector. Particle velocity is found from the transit time of the particle through the detector or, more accurately, from the transit time of the particle from the detector input (leading edge of rectangular pulse) to impact on the target (flight path length = 1.42 meters in this case). Particle parameters may be calculated by invoking the principle of conservation of energy on the accelerated particle and proceeding in the following manner (MKS system):

$$\frac{1}{2} mv^2 = Q\ Va$$

$$Q = \frac{C}{g} Vo$$

$$v = \frac{L}{t}$$

$$r = \sqrt[3]{\frac{3m}{4\pi\rho}}$$

where;

m = particle mass,

v = particle velocity,

Q = particle charge,

Va = total accelerating potential,

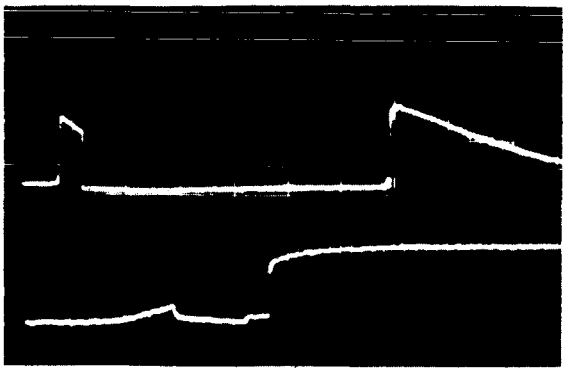

IMPACT VELOCITY: 1.16 km/s
MASS: 1.72×10^{-13} kg
RADIUS: 2.51×10^{-6} m
COLLECTED CHARGE: 3.0×10^{-14} C

(a)

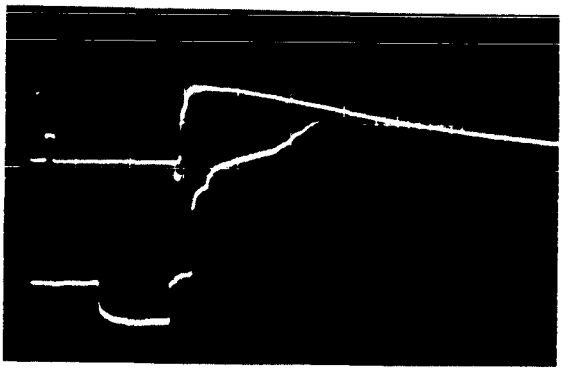

IMPACT VELOCITY: 5.76 km/s
MASS: 1.06×10^{-15} kg
RADIUS: 4.60×10^{-7} m
COLLECTED CHARGE: 1.71×10^{-13} C

(b)

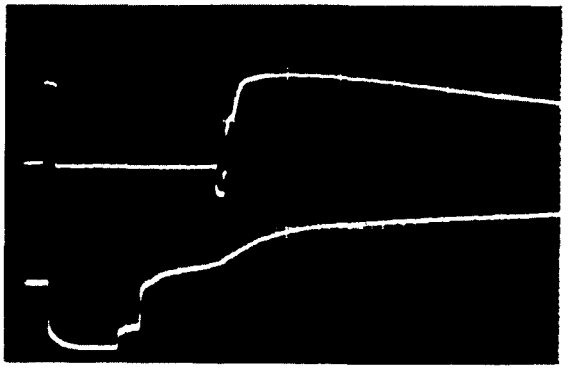

IMPACT VELOCITY: 8.85 km/s
MASS: 3.70×10^{-16} kg
RADIUS: 3.23×10^{-7} m
COLLECTED CHARGE: 2.69×10^{-13} C

(c)

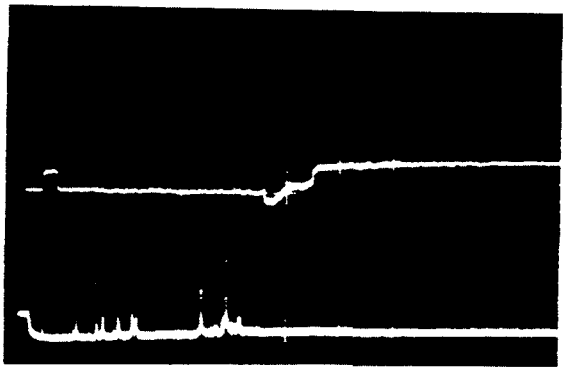

IMPACT VELOCITY: 17.1 km/s
MASS: 2.31×10^{-17} kg
RADIUS: 1.28×10^{-7} m
COLLECTED CHARGE: 7.7×10^{-14} C

(d)

Figure 3-4. Signal Response for Various LaB_6 Particle Impacts on a Tantalum Target. The upper trace, in each case, is the sum of the particle charge detector, target, and collected ion signals. The lower trace, in each case, is the sum of the target and PMT signals.

C = particle charge detector input capacitance,

g = detector amplifier gain,

Vo = particle detector signal output amplitude (rectangular pulse on upper trace),

L = measured flight path length,

t = transit time over flight path length (measured on upper trace of photograph),

r = particle equivalent radius, if spherical,

ρ = density of particle material.

Referring again to Figure 3-4a, which is a 1.16 km/sec impact, the lower trace is seen to begin prior to particle impact on the target which is accomplished by the trigger pulse from the particle selection system. The positive going ramp in this photograph is caused by the positive charge on the particle being induced on the target prior to actual impact of the particle. Impact occurs at the time the negative step appears at the end of the positive ramp. The negative step gives the time of impact from which all ion transit times are measured. Following particle impact in Figure 3-4a, two positive going steps may be easily seen. The first small step is caused by the arrival of sodium ions (Na^+) at the collector while the second or large step is the arrival of potassium ions (K^+). A third elements signal may be seen at the top of the large step which is either $(K^{41})^+$, Ca^+, or a combination of both. The total charge collected may be measured from the total amplitude of the collector signal on either lower or upper trace.

Figure 3-4b shows an impact at 5.76 km/sec. On the lower trace, the collector signal shows several more distinquishable steps. After the first step (Na^+), a small Si^+ signal has appeared followed by a large $(K^{39})^+$ signal, a small [$(K^{41})^+$, Ca^+] signal, a new small step at mass 54-56 AMU which has not been positively identified, and finally, a slow rising step as the signal goes off scale. The slow step is characteristic of essentially all LaB_6 impacts below about 10 km/sec. The source of this slow signal is not known. It corresponds to an ion mass in the 180-

210 range and may be tantalum or the LaB_6 molecule.

Figure 3-4c is an impact at 8.85 km/sec and is essentially identical in character to that in Figure 3-4b.

Figure 3-4d shows a collector signal current waveform from a higher velocity impact (17.1 km/sec). This photograph illustrates the exceptional improvement in the output spectrum as the velocity increases to the 20 km/sec range. Very fine resolution is illustrated here and is representative of a high velocity impact with a one meter TOF range. The observed elements or mass numbers, in increasing order of mass, are as follows: H, C, Na, Si,(mass 39-41), (mass 53-56), La, Ta, and mass 205 which is correct for the LaB_6 molecule.

The LaB_6 impact data which were recorded as integrated collector signals (such as Figure 3-4a, b, c) were examined in detail to find both the amplitude and transit time of each distinquishable step. These signals were then used to compute the total charge contained in each step and the mass in AMU of the ion group which produced the step. These data were then split into four velocity groups; 0-3 km/sec, 3-6 km/sec, 6-9 km/sec, and 9 km/sec and above. The charge collected in a given AMU number was then summed over all impacts in each velocity group. Figures 3-5, 3-6, 3-7, and 3-8 are the results obtained.

Figure 3-5 is the 0-3 km/sec group and Figure 3-6 is the 3-6 km/sec group. In the lowest velocity group, sodium and potassium-calcium are esentially the only signals present. A sizeable number of other mass numbers are obtained but either infrequently or of low amplitude. As can be seen in this histogram which plots total collected charge in each atomic mass group, substantially all the charge is contained in these two groups. In Figure 3-6, the 3-6 km/sec group, substantially all the charge is still carried in the 23, 39-41 AMU groups, however, sizeable signals may now be found at mass 28 (Si), mass 53-57 (unknown), and mass 180-200 (most likely tantalum and tantalum monoxide (TaO) or LaB6). The large spread in signals in the 180-200 AMU range is caused by the slow risetime nature of the waveform described earlier.

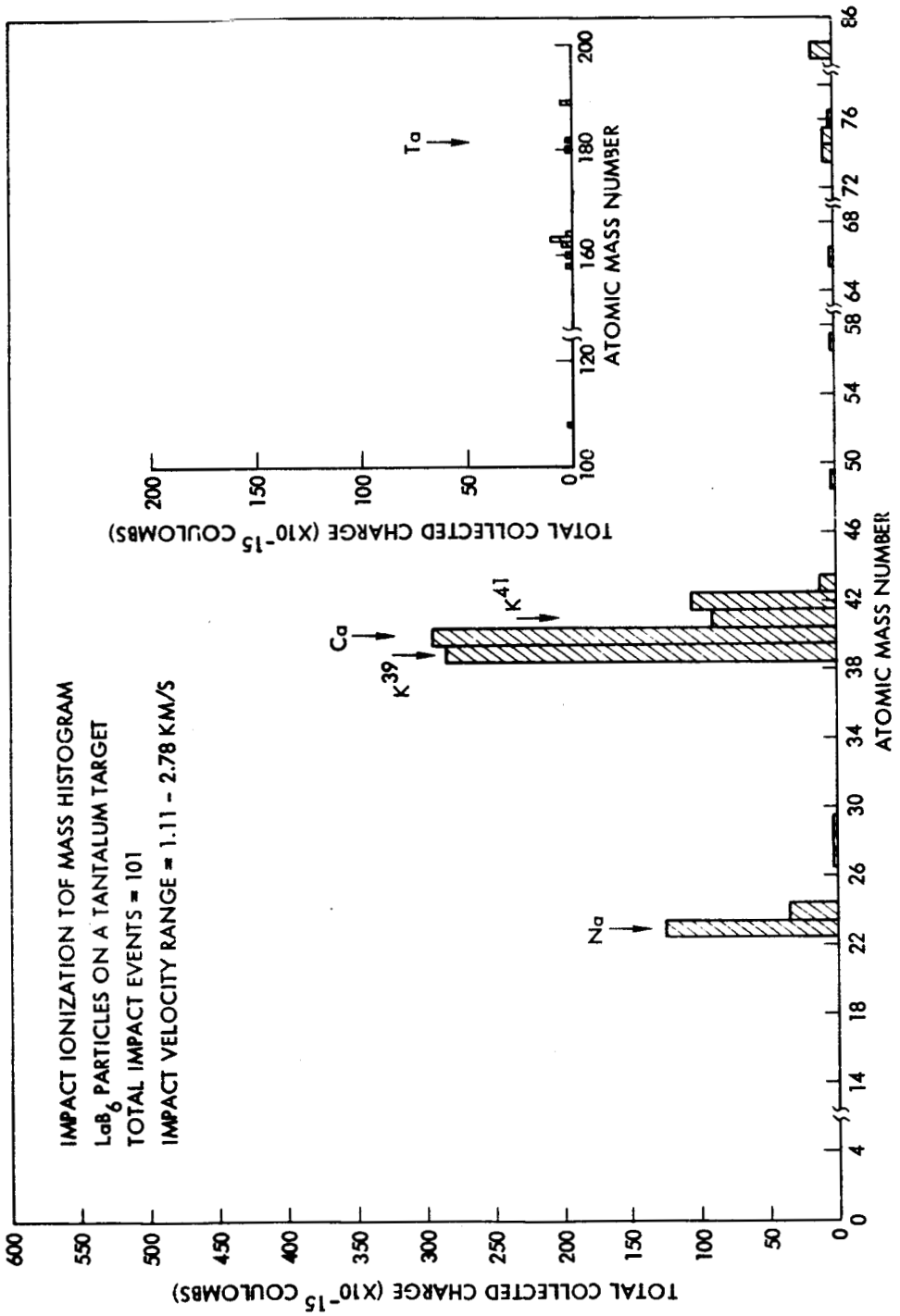

Figure 3-5. Mass Histogram of Collected Charge for LaB_6 Particle Impacts on a Ta Target, using ion TOF. Particle impact velocity range is 1.11 - 2.73 km/s.

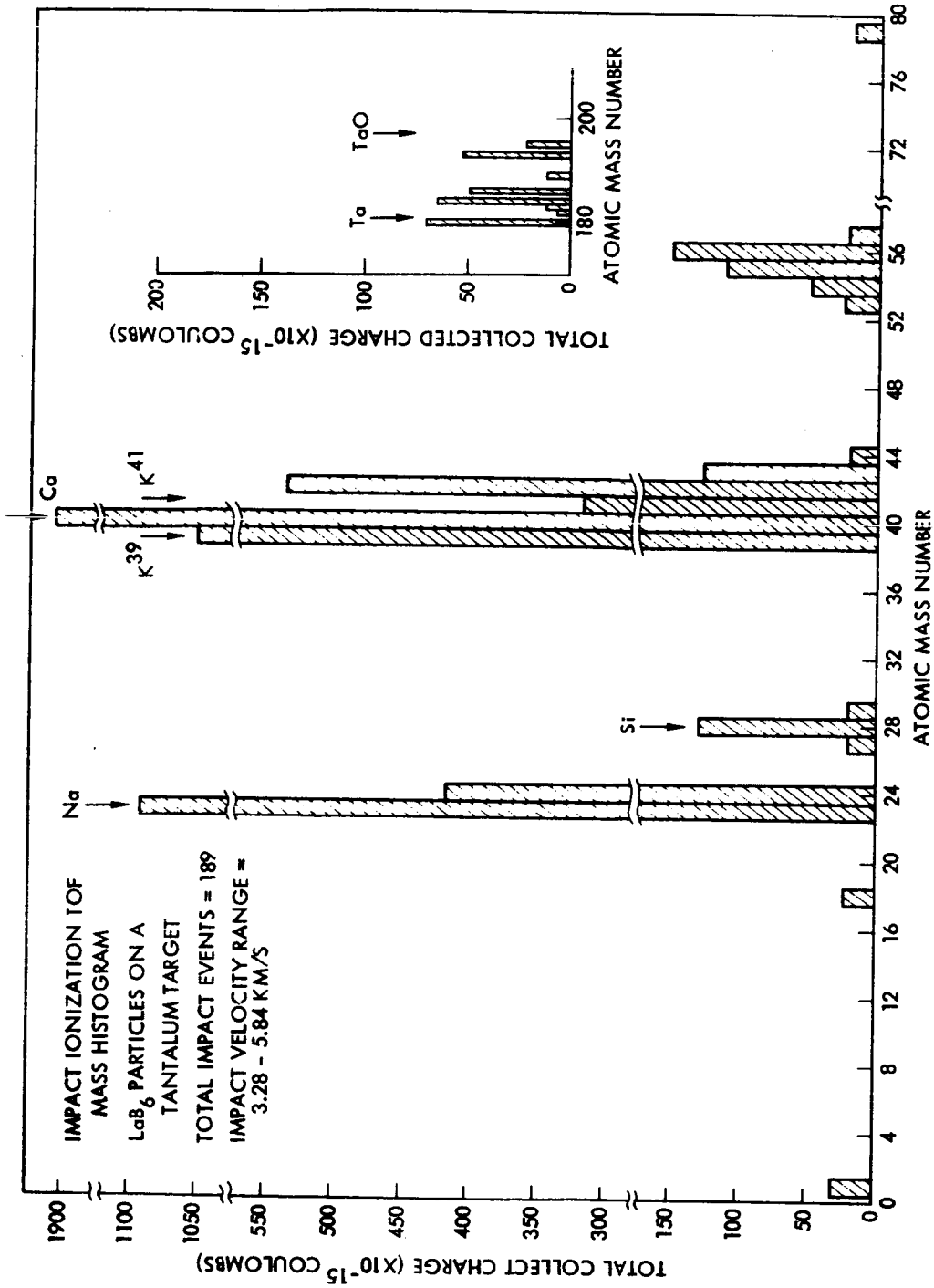

Figure 3-6. Mass Histogram of Collected Charge for LaB_6 Particle Impacts on a Ta Target, using ion TOF. Particle impact velocity range is 3.2 - 5.84 km/s.

Figure 3-7 and 3-8 shows the results obtained for the 6-9 km/sec, and 9 km/sec and up group. These histograms are not materially different from that in Figure 3-6 (3-6 km/sec group) except in Figure 3-8 (9 km/sec and over) carbon has appeared and also several low amplitude signals have shown up around mass 140 which is assumed to be lanthanum. Both boron and lanthanum are noteably absent from these histograms in significant quantities. The low signal levels for these two elements are believed to be for the following reasons: (1) The LaB_6 molecule contains six boron atoms which surround the much larger lanthanum atom. In order to obtain a free lanthanum atom, which could then be easily ionized, all six boron atoms must be stripped away. It is believed that the energy involved in doing this is sufficiently large to significantly reduce the number of lanthanum atoms available for thermal ionization. (2) On the other hand, freeing one or boron atoms should occur easily; however, this atom has an 8.30 eV ionization potential and is therefore not expected to be appreciably ionized at low impact velocities.

The total impact ionization charge leaving the target was measured for each of the recorded impact events. Figure 3-9 shows the results obtained when these data are normalized to the mass of the impacting particle. It was assumed that the plotted data could best be described by an equation of the form $Q_T/m_p = Kv^{\alpha}$. The line shown on Figure 3-9 is the estimated best fit to the plotted data. The equation which describes the line drawn was found to be $Q_T/m_p = (.060)\ v^{4.48}$ where Q_T/m_p will be in coulombs per kilogram when v is expressed in km/sec.

A second plot was made from the total charge measured in the 39-41 AMU group of ions. When normalized to particle mass, the plot in Figure 3-10 is obtained. The data are seen to scatter more than the total charge data of Figure 3-9; however, the curve for the estimated best fit does not differ substantially from that for the total. The equation obtained for the curve is $Q_c/m_p = (.013)\ v^{4.45}$ which differs from that found for the total only in the value of the constant.

3.3.2 Iron Particle Impacts

Impact ionization signals were recorded for iron particle impacts on tantalum over essentially the same velocity range used for the previous

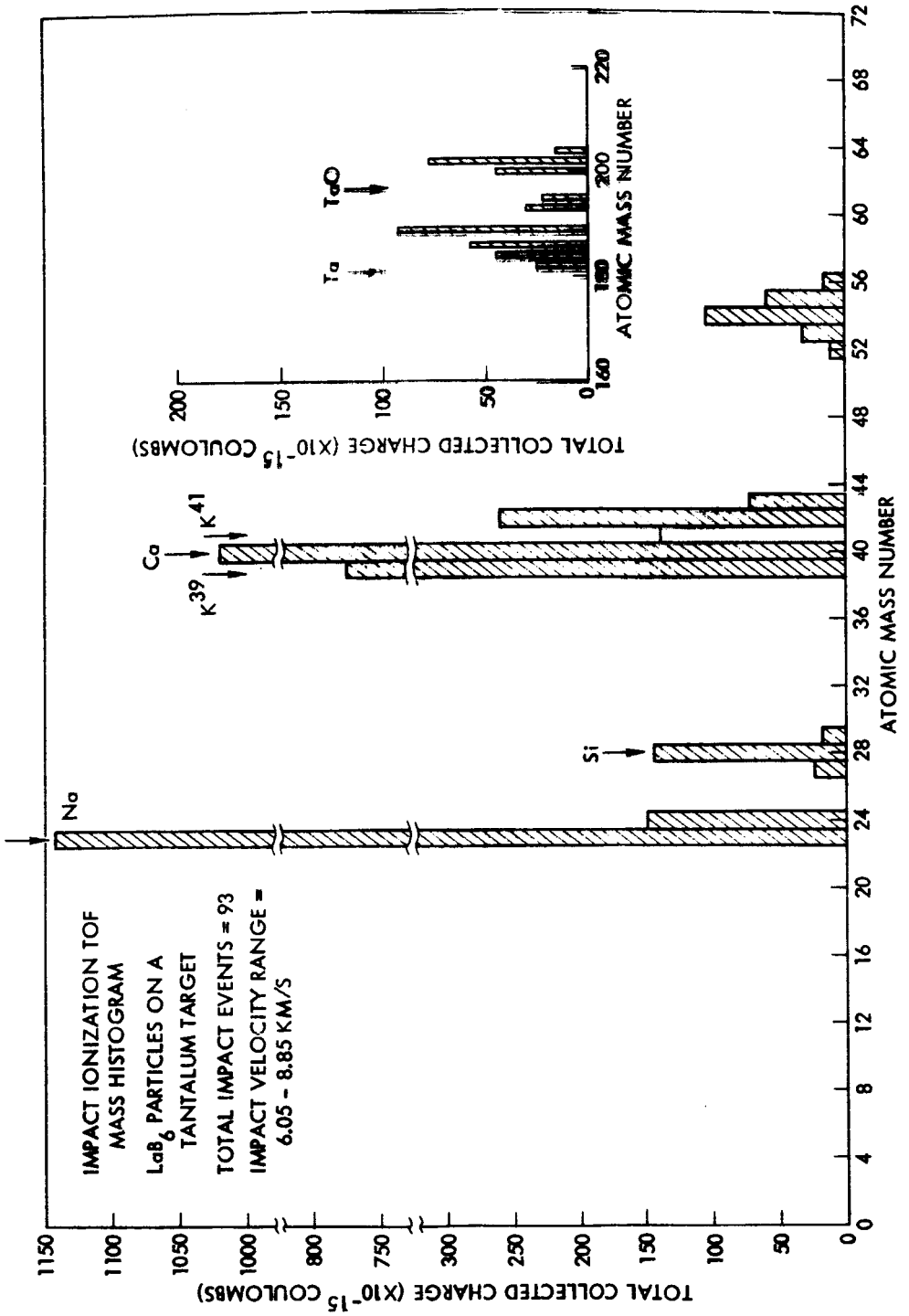

Figure 3-7. Mass Histogram of Collected Charge for LaB_6 Particle Impacts on a Ta Target, using ion TOF. Particle impact velocity range is 6.05 - 8.85 km/s.

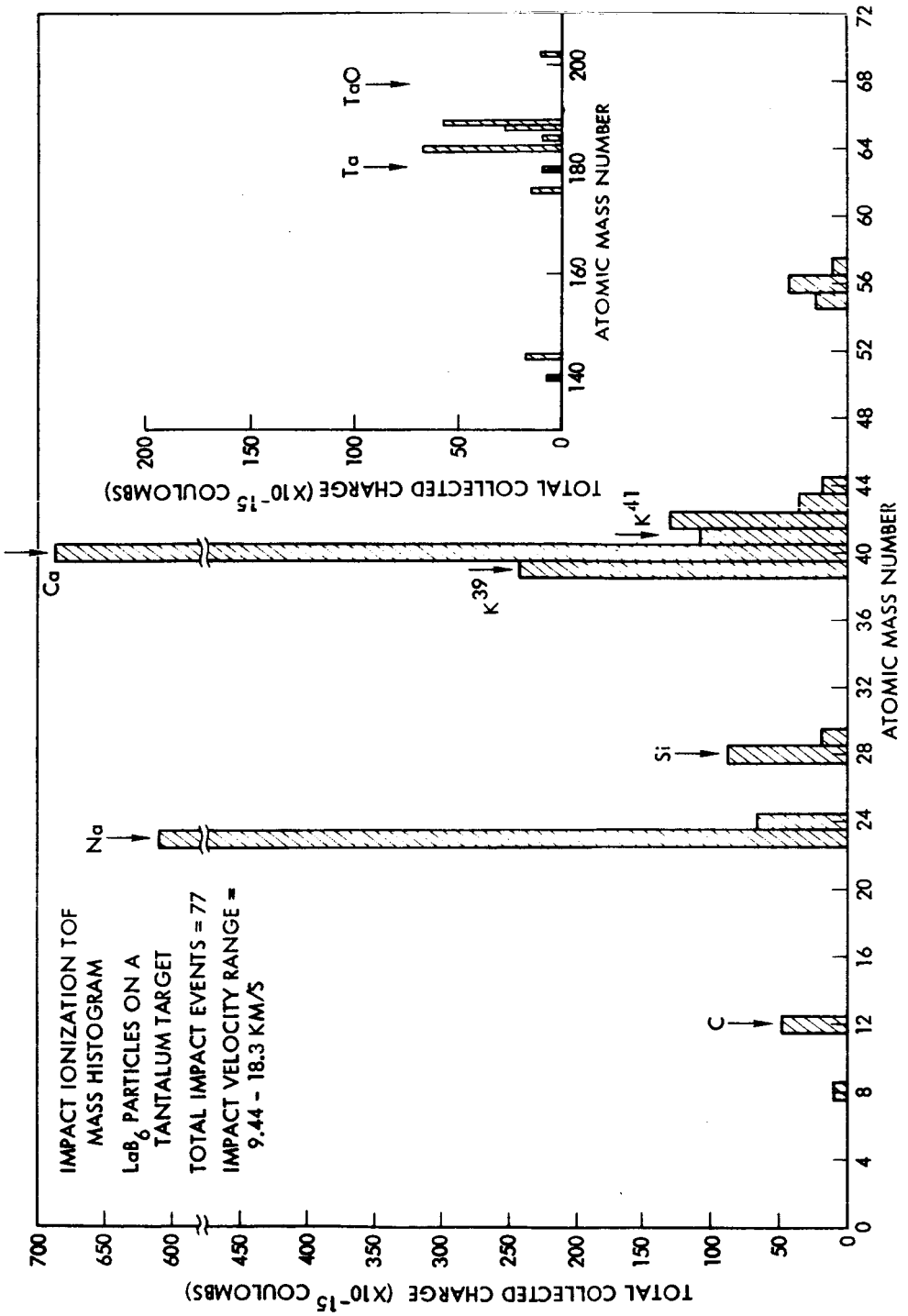

Figure 3-8. Mass Histogram of Collected Charge for LaB_6 Particle Impacts on a Ta Target, using ion TOF. Particle impact velocity range is 9.44 - 18.3 km/s.

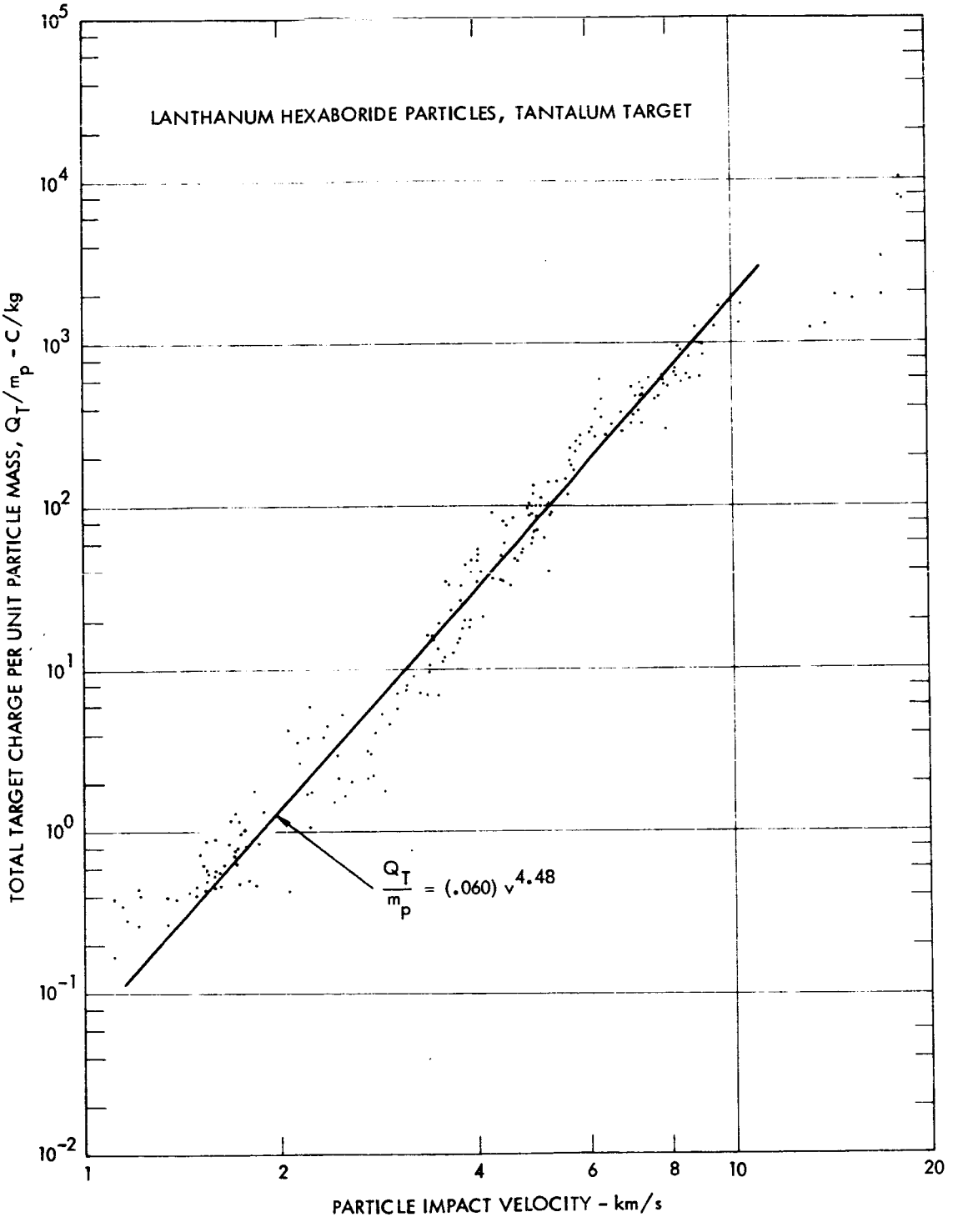

Figure 3-9. Total Target Charge Per Unit Particle Mass Q_T/m_p vs Particle Impact Velocity: LaB_6 Particles, Ta Target.

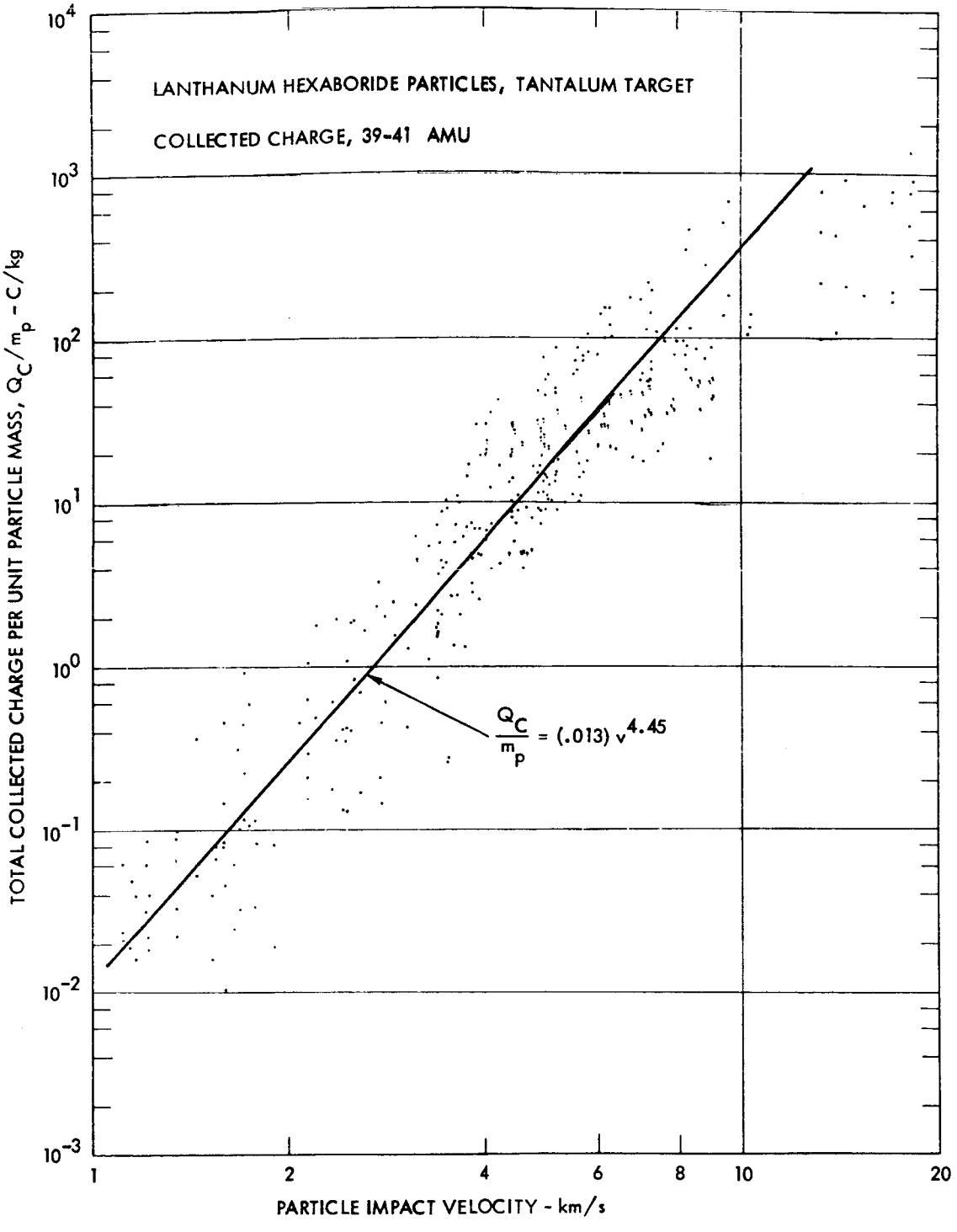

Figure 3-10. Total Collected Charge (39-41 AMU Mass Group) Per Unit Particle Mass Q_c/m_p vs Particle Impact Velocity: LaB_6 Particles, Ta Target.

LaB_6 impacts. In this case, the Van de Graaff accelerator and the linear accelerator were both used for impact data acquisition. The linear accelerator was used in order to check on any possible mass effects which might exist for the impact ionization process.

Figure 3-11 shows four oscilloscope photographs that are representative of the iron particle impacts obtained. In Figure 3-11a, a low velocity (1.33 km/sec) impact signal is shown. The signals displayed are the same as described for the LaB_6 data. The upper trace shows the sum of the particle charge detector signal, the target signal, and the integrated collector signal. The lower trace shows the sum of the target signal and the integrated collector signal but at a higher sweep speed (5 microseconds/division) than the upper trace. Three separate ion groups are distinquishable on the lower trace. The masses of the three groups were found to be 23, 39, and 75 AMU. Sodium and potassium are present as for the other low velocity impacts, however, the mass 75 group is new and has not been identified. It was observed only for impacts below 3 km/sec.

Figure 3-11b illustrates an impact signal at 3.37 km/sec. This particular event shows only sodium and potassium and is representative of most of the events recorded in the 3-6 km/sec range.

Figure 3-11c is an event at 6.46 km/sec. Here three ion groups are seen quite prominently. They were identified as sodium, potassium, and iron.

Figure 3-11d shows an event at 7.75 km/sec for an iron particle which was accelerated by the linear accelerator. The signal on the upper trace is the sum of the signal from the linear accelerator particle position detector, and the target signal, and the integrated collector signal. The same ion mass groups are observed here as for the 6.46 km/sec impact in Figure 3-11c; sodium, potassium, and iron. However, the mass of the particle in this case is two orders of magnitude greater ($m = 2.08 \times 10^{-14}$ kg in (d) vs $m = 2.92 \times 10^{-16}$ kg in (c)).

The total charge collected in each ion group was measured for each impact event recorded. The data were separated into four velocity

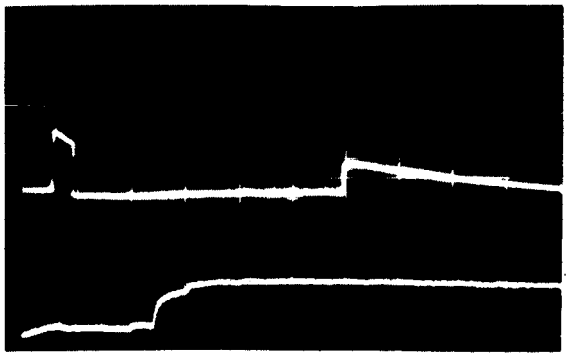

IMPACT VELOCITY: 1.33 km/s
MASS: 1.19×10^{-13} kg
RADIUS: 1.54×10^{-6} m
COLLECTED CHARGE: 1.16×10^{-14} C

(a)

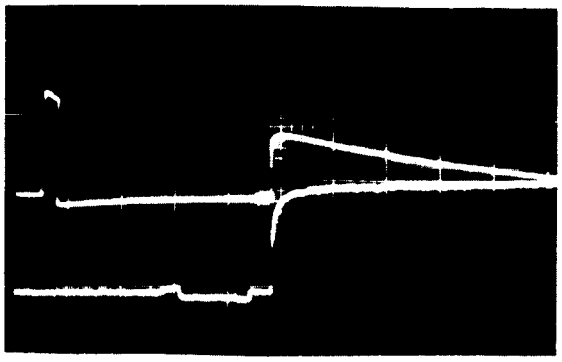

IMPACT VELOCITY: 3.37 km/s
MASS: 6.29×10^{-15} kg
RADIUS: 5.76×10^{-7} m
COLLECTED CHARGE: 4.97×10^{-14} C

(b)

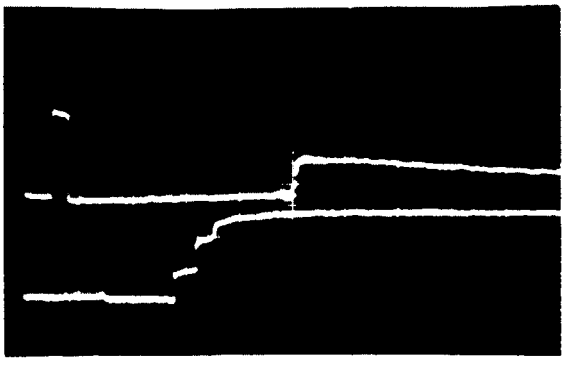

IMPACT VELOCITY: 6.46 km/s
MASS: 2.92×10^{-16} kg
RADIUS: 2.07×10^{-7} m
COLLECTED CHARGE: 1.02×10^{-14} C

(c)

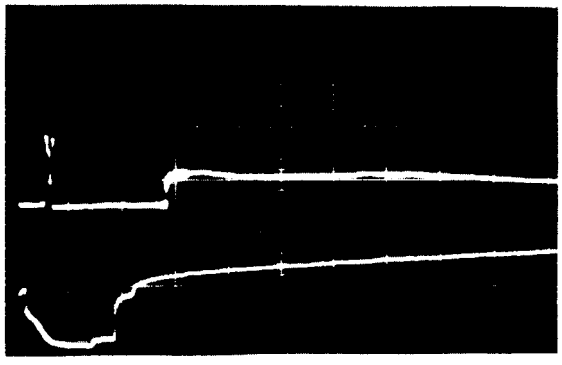

IMPACT VELOCITY: 7.75 km/s
MASS: 2.08×10^{-14} kg
RADIUS: 8.58×10^{-7} m
COLLECTED CHARGE: 6.45×10^{-14} C

(d)

Figure 3-11. Signal Response for Various Carbonyl Iron Particle Impacts on a Tantalum Target. The upper trace in (a), (b), and (c) is the sum of the particle charge detector and the integrated PMT signal. The upper trace in (d) is the sum of the particle position detector and the integrated PMT signal. The lower trace in each case is the sum of the target signal and the integrated PMT signal.

groups, 0-3 km/sec, 3-6 km/sec, 6-9 km/sec, and 9 km/sec and above. The collected charge in a given AMU number was then summed over all impacts for each velocity group. These data are shown as histograms in Figures 3-12, 3-13, 3-14, and 3-15. In the 0-3 km/sec, 3-6 km/sec, and 6-9 km/sec only three ion groups are generally observed. They are sodium, potassium, and iron with iron being a weak or low-level signal in all cases, especially in the 0-3 km/sec group. For the 9.47 km/sec - 32.0 km/sec group shown in Fiugre 3-15, iron has become a much larger fraction of the total collected charge. Other mass groups are also observed for these impacts. Hydrogen, lithium, carbon, silicon, tantalum, and tantalum oxide are present as may be seen from the figure.

The total collected charge for the carbonyl iron impacts were measured and normalized to the mass of the impacting particle. These normalized charge data were plotted against particle impact velocity and are shown in Figure 3-16. Here the data acquired using the Van de Graaff accelerator have been coded differently from that acquired using the linear accelerator in order to see if a mass effect exists for impact ionization at these velocities. The two data groups are quite clearly separated in this graph which shows that an incorrect normalization factor has been used. If impact ionization was proportional to mass then both data groups would have the same amplitude and slope on this graph. This is clearly not the case; hence, impact ionization does not go directly as mass of the impacting particle.

The two lines drawn on Figure 3-16 are the estimated best fit for the plotted data. The equation found for the curves were $Q_c/m_p = (0.44)v^{3.97}$ for the upper or Van de Graaff accelerator data group and $Q_c/m_p = (.025)v^{2.6}$ for the lower or linear accelerator data group.

In order to obtain a quantitative feeling for the magnitude of the mass exponent for production of impact ionization, the charge collected at 10.0 $\pm$ km/sec were plotted as a function of the mass of the impacting particle. The result obtained is shown in Figure 3-17. In this figure the collected charge datum points for the Van de Graaff and linear accelerator data groups are separated by approximately two orders of magnitude in particle mass. A least-squares linear regression was per-

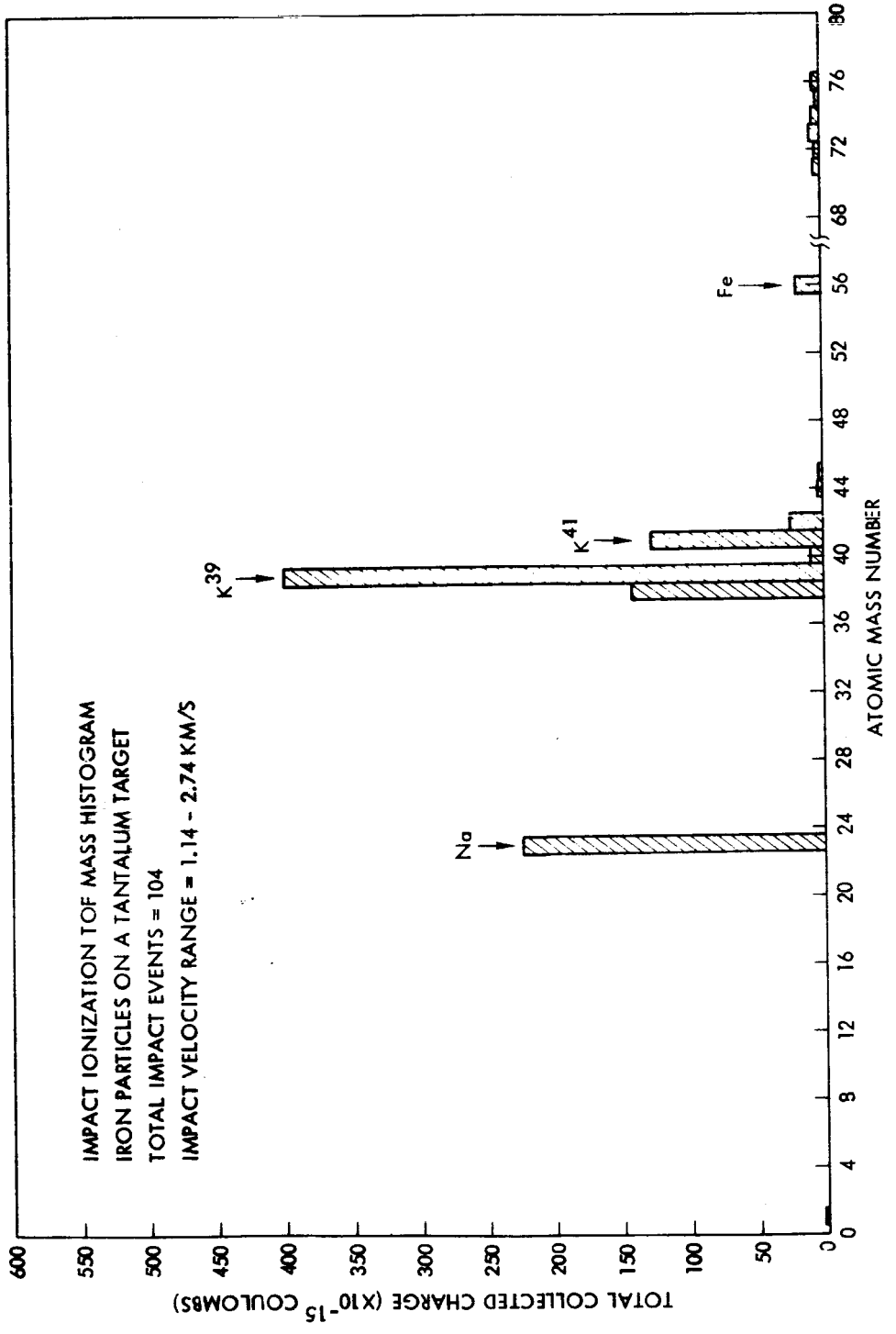

Figure 3-12. Mass Histogram of Collected Charge for Carbonyl Iron Particles on a Ta Target, using ion TOF. Particle impact velocity range is 1.14 - 2.74 km/s.

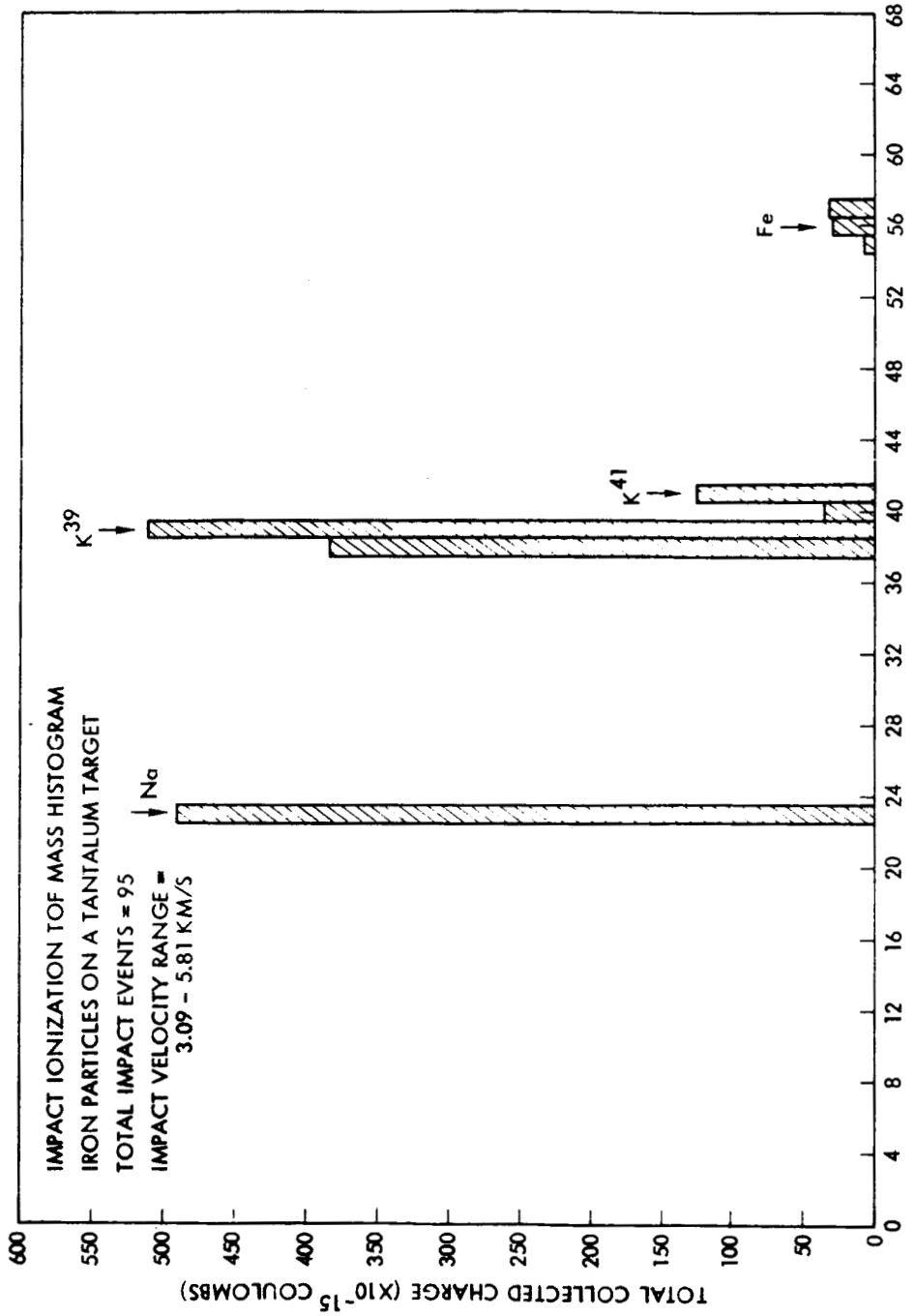

Figure 3-13. Mass Histogram of Collected Charge for Carbonyl Iron Particles on a Ta Target, using ion TOF. Particle impact velocity range is 3.09 - 5.81 km/s.

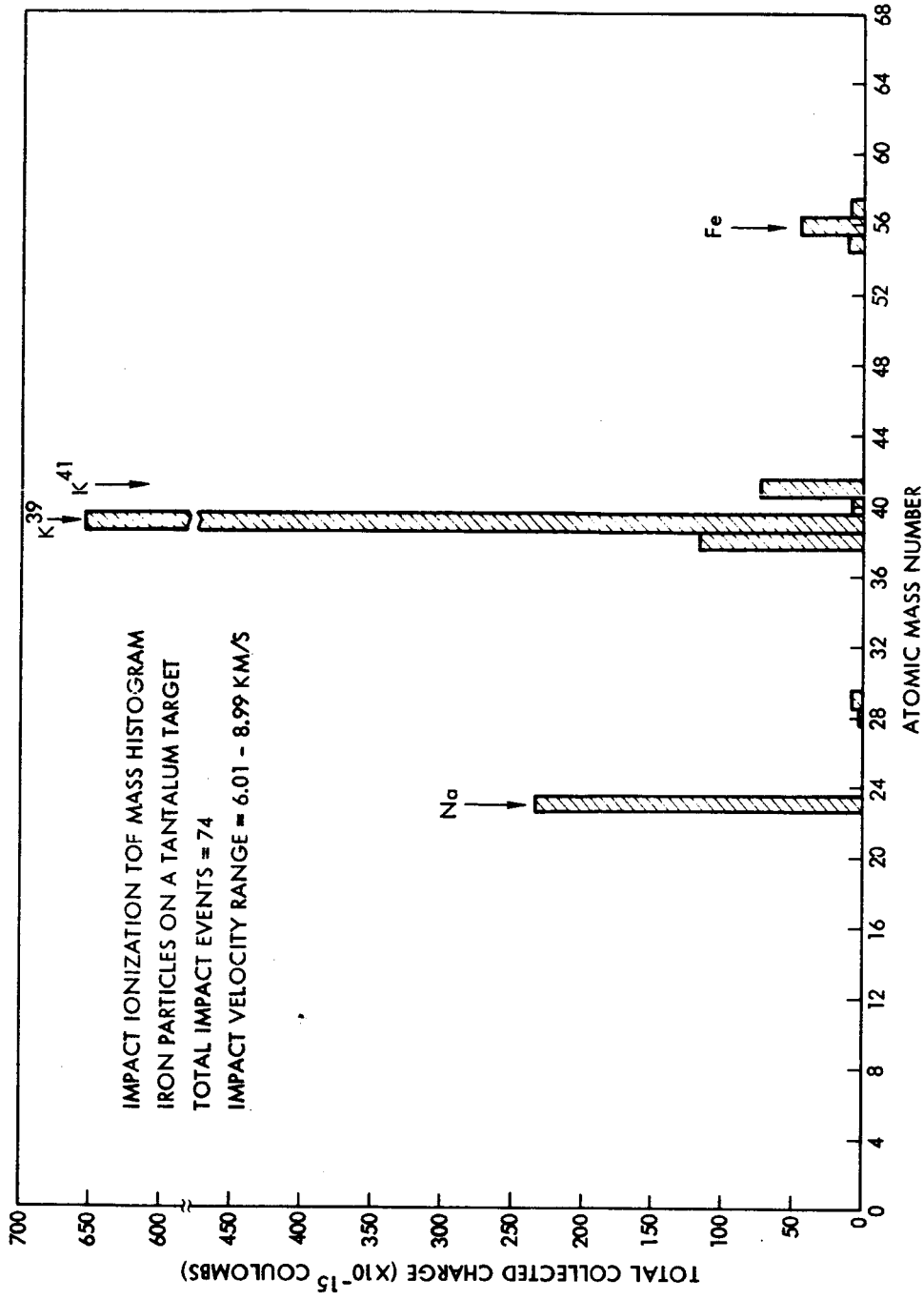

Figure 3-14. Mass histogram of Collected Charge for Carbonyl Iron Particles on a Ta Target, using ion TOF. Particle impact velocity range is 6.01 - 8.99 km/s.

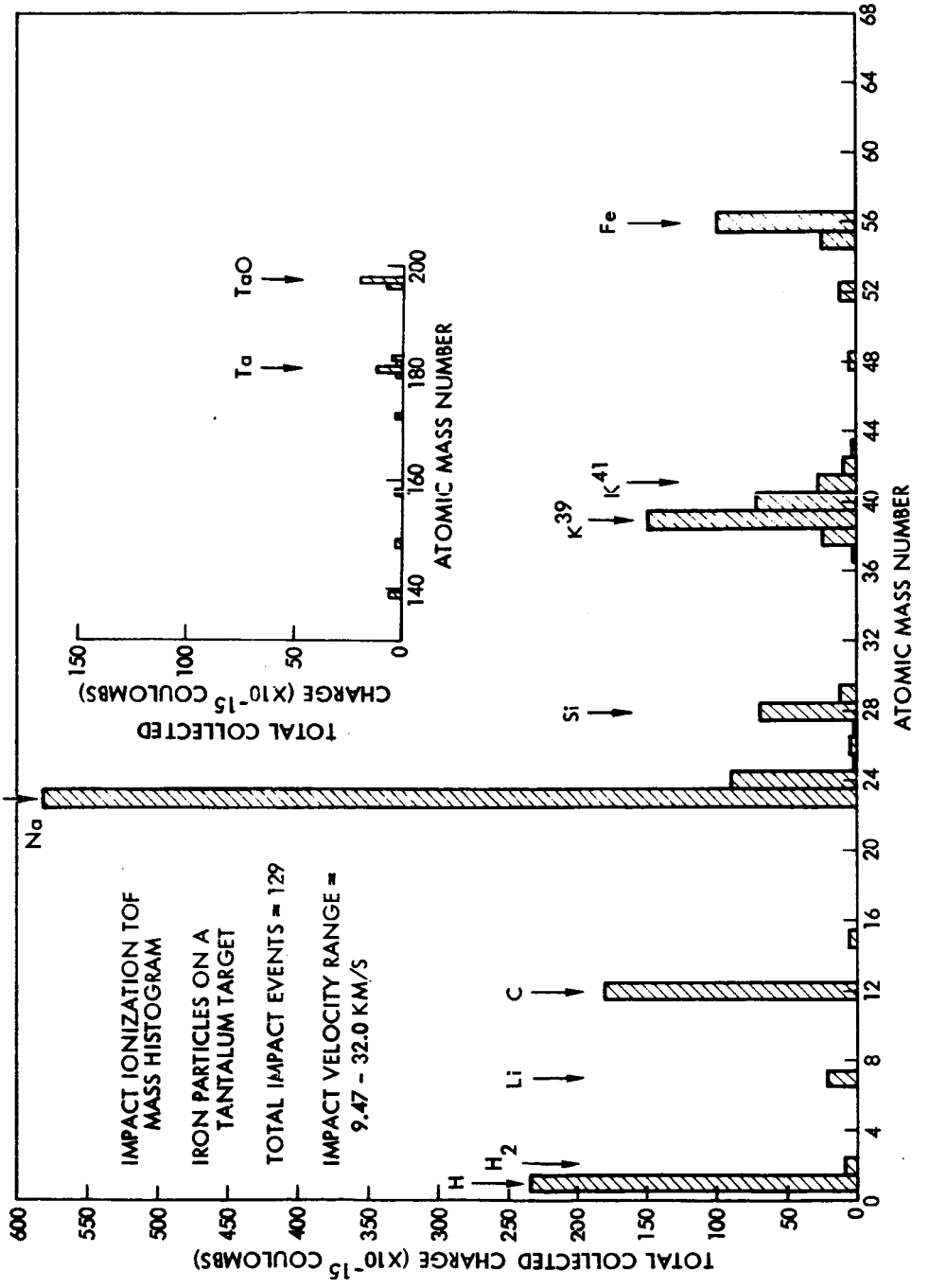

Figure 3-15. Mass Histogram of Collected Charge for Carbonyl Iron Particles on a Ta Target, using ion TOF. Particle impact velocity range is 9.47 - 32.0 km/s.

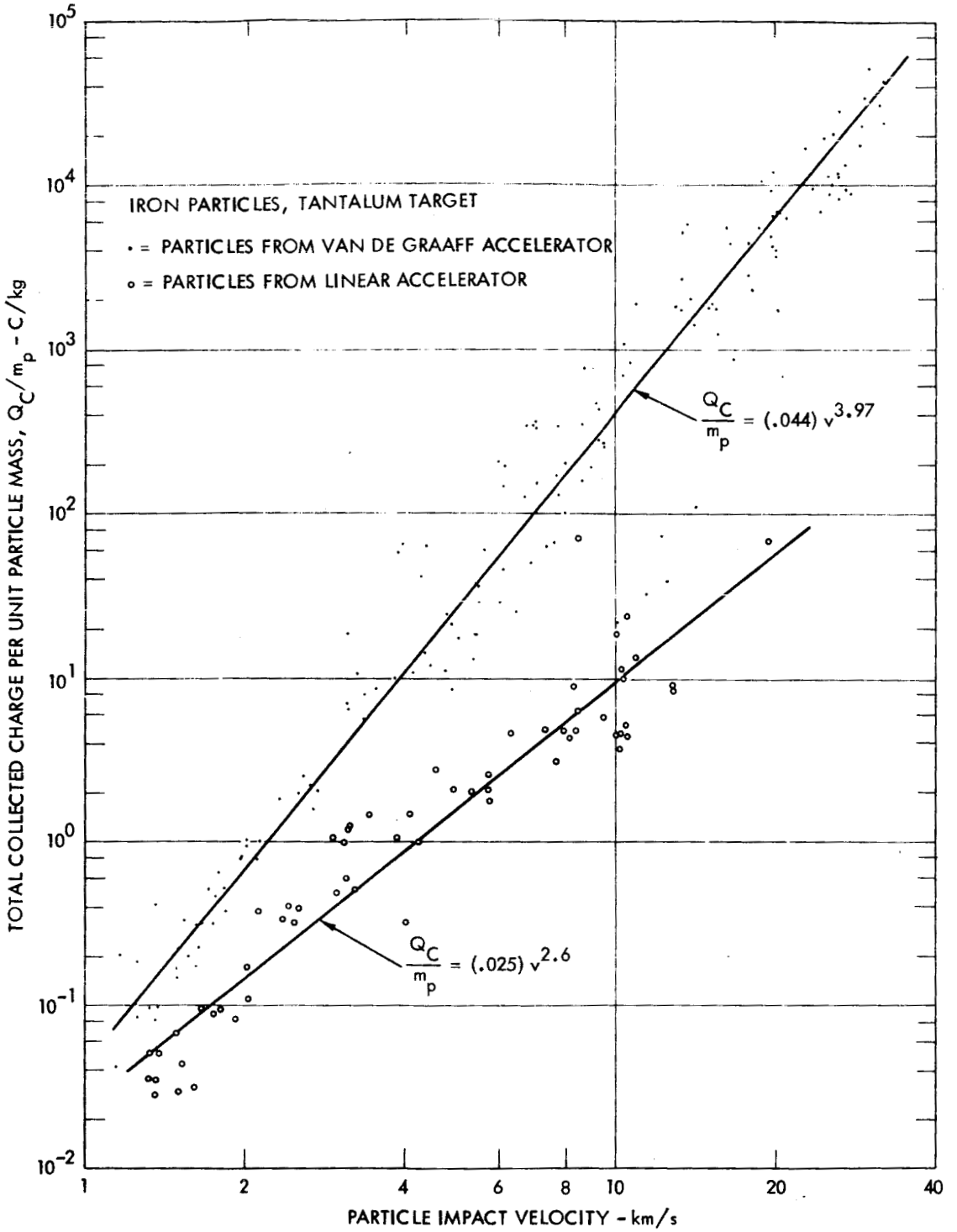

Figure 3-16. Total Collected Charge Per Unit Particle Mass Q_c/m_p vs Particle Impact Velocity: Carbonyl Iron Particles, Ta Target.

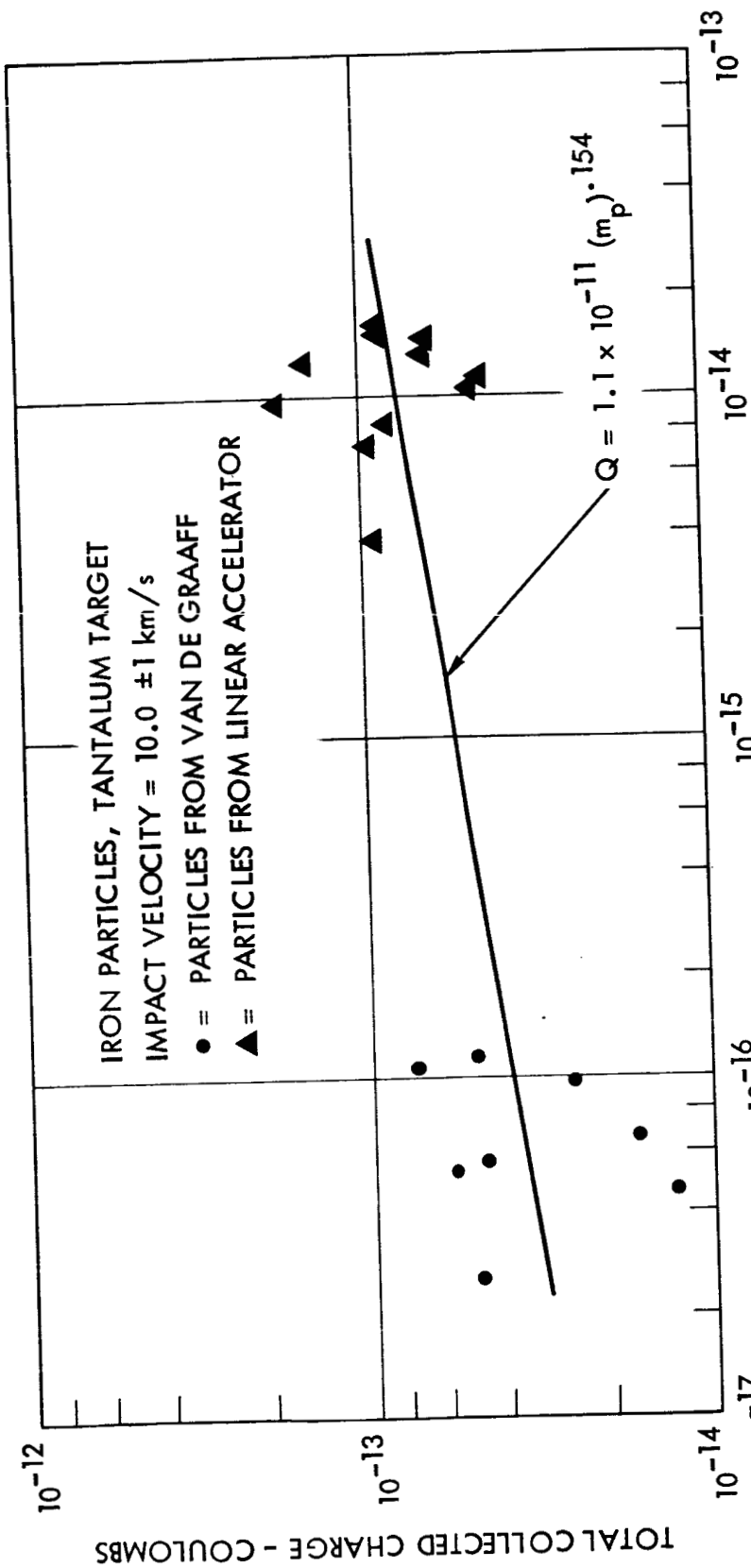

Figure 3-17. Total Collected Charge vs Particle Mass: Carbonyl Iron Particles, Ta Target. Impact velocity is 10 ± 1 km/s.

formed on the plotted data to obtain the line shown on the figure. Although the number of data points in each group are limited, the two groups are sufficiently far apart in mass so that the exponent of mass may be extracted from these data. An equation was obtained for the least-squares fit to the plotted data which is

$$Q = 1.1 \times 10^{-11} (m_p)^{.154} \quad .$$

The above equation shows an extremely strong mass dependence for the velocity and impact parameters used for the data from which the equation was derived. A similar plot was attempted from the relatively few datum points at $1.5 \pm .15$ km/sec; however, the mass difference between the two data groups is only a factor of five at this velocity. The scatter in the collected charge data was too large to permit a mass dependence to be determined.

The much smaller mass difference at the low velocities is the reason the two data groups converge at one km/sec in Figure 3-14. A constant difference in the mass ratios of the two groups would have established parallel trends in this figure.

3.3.3 Aluminum Particle Impacts

Aluminum has the lowest ionization potential of the three particle materials tested on this program. The character of the ionization signal also changes substantially to reflect the lower ionization potential of the aluminum. Figure 3-18 shows four oscilloscope photographs which are representative of the type signals obtained over the velocity range covered in the tests. The collector signal on the lower trace in these examples is the time history of the ion current arriving at the collector. Figure 3-18a is for an impact at 1.3 km/sec. The collector signal on the lower trace shows three prominent current spikes which correspond to sodium, potassium, and mass 74 which has not been positively identified. The impacts down near one km/sec are the only cases where aluminum failed to show up as an identifiable element on the collector signal.

Figure 3-18b is the signal obtained for a 3.36 km/sec impact. The signals seen on the lower trace correspond to, in increasing order of

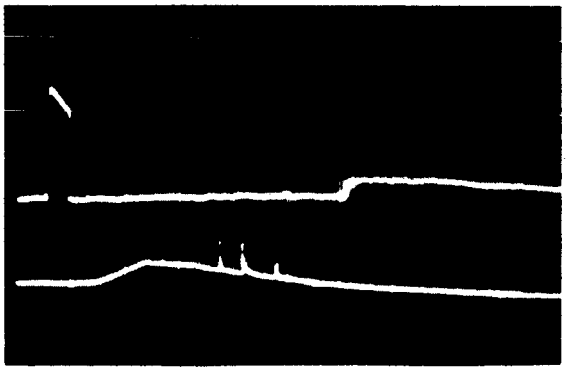

IMPACT VELOCITY: 1.30 km/s
MASS: 1.75×10^{-13} kg
RADIUS: 2.49×10^{-6} m
COLLECTED CHARGE: 2.06×10^{-14} C

(a)

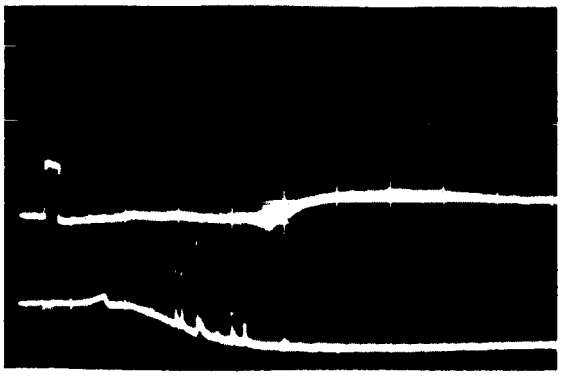

IMPACT VELOCITY: 3.36 km/s
MASS: 1.71×10^{-14} kg
RADIUS: 1.15×10^{-6} m
COLLECTED CHARGE: 7.11×10^{-14} C

(b)

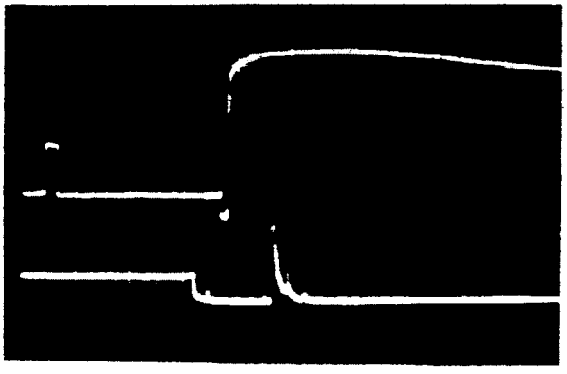

IMPACT VELOCITY: 8.68 km/s
MASS: 8.24×10^{-16} kg
RADIUS: 7.52×10^{-7} m
COLLECTED CHARGE: 7.45×10^{-13} C

(c)

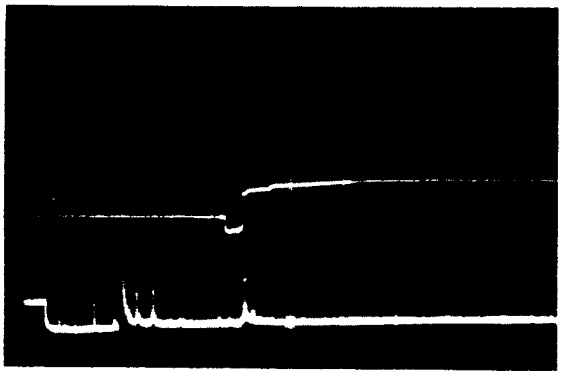

IMPACT VELOCITY: 20.9 km/s
MASS: 5.71×10^{-17} kg
RADIUS: 1.72×10^{-7} m
COLLECTED CHARGE: 4.50×10^{-13} C

(d)

Figure 3-18. Signal Response for Various Aluminum Particle Impacts on a Tantalum Target. The upper trace in each case is the sum of particle charge detector signal, target signal, and collector signal. The lower trace is the sum of the target signal and the PMT current waveform.

mass, sodium, aluminum, potassium, mass 74, and mass 90.

Figure 3-18c shows the signal from an impact at 8.68 km/sec. In increasing order the current signals seen on the lower trace represent hydrogen (small), sodium (very small), aluminum (very large), potassium (small), and mass 54. One sees that the aluminum signal is by far the most prominent signal for this impact.

Figure 3-18d illustrates the results of an impact at 20.9 km/sec. As these higher velocities are reached the collector signal is seen to change substantially in the number of elements which are detected. In this photograph (lower trace) major current spikes are seen which have been identified as H, C, Al (very large spike), K, mass 54, and Ta. Minor peaks are seen which have the following calculated mass numbers: (2), (23), (41), and (197) which is believed to be tantalum oxide (TaO).

The total collected charge in each measurable ion mass group was found as for the previous particle materials. The acquired data was split into the same four velocity ranges (0-3 km/sec, 3-6 km/sec, 6-9 km/sec, 9 km/sec and up) used previously. The collected charge found for each atomic mass unit was summed over all impacts in each velocity group. The resulting plots are shown in Figures 3-19, 3-20, 3-21, and 3-22. These data require no further explanation since they are in the same format as the preceding two groups. It is worth noting that aluminum is quite prominent in these histograms.

The total collected charge for each impact was also measured for the aluminum particle impacts. These data were normalized to the impacting particle mass and were plotted as a function of impact velocity. The results are shown in Figure 3-23. Here again a line has been drawn for the estimated best fit to the plotted data. The equation for the line is $Q_c/m_p = (.038)v^{3.89}$ where Q_c/m_p will be in coulombs/kg when v is expressed in km/sec.

3.3.4 Discussion of Ionization Data Relative to the Proposed Plasma Model

It is apparent from the data presented earlier that the alkali materials, sodium and potassium, are by far the most prominent ionized species at the low impact velocities. The presence of these two elements

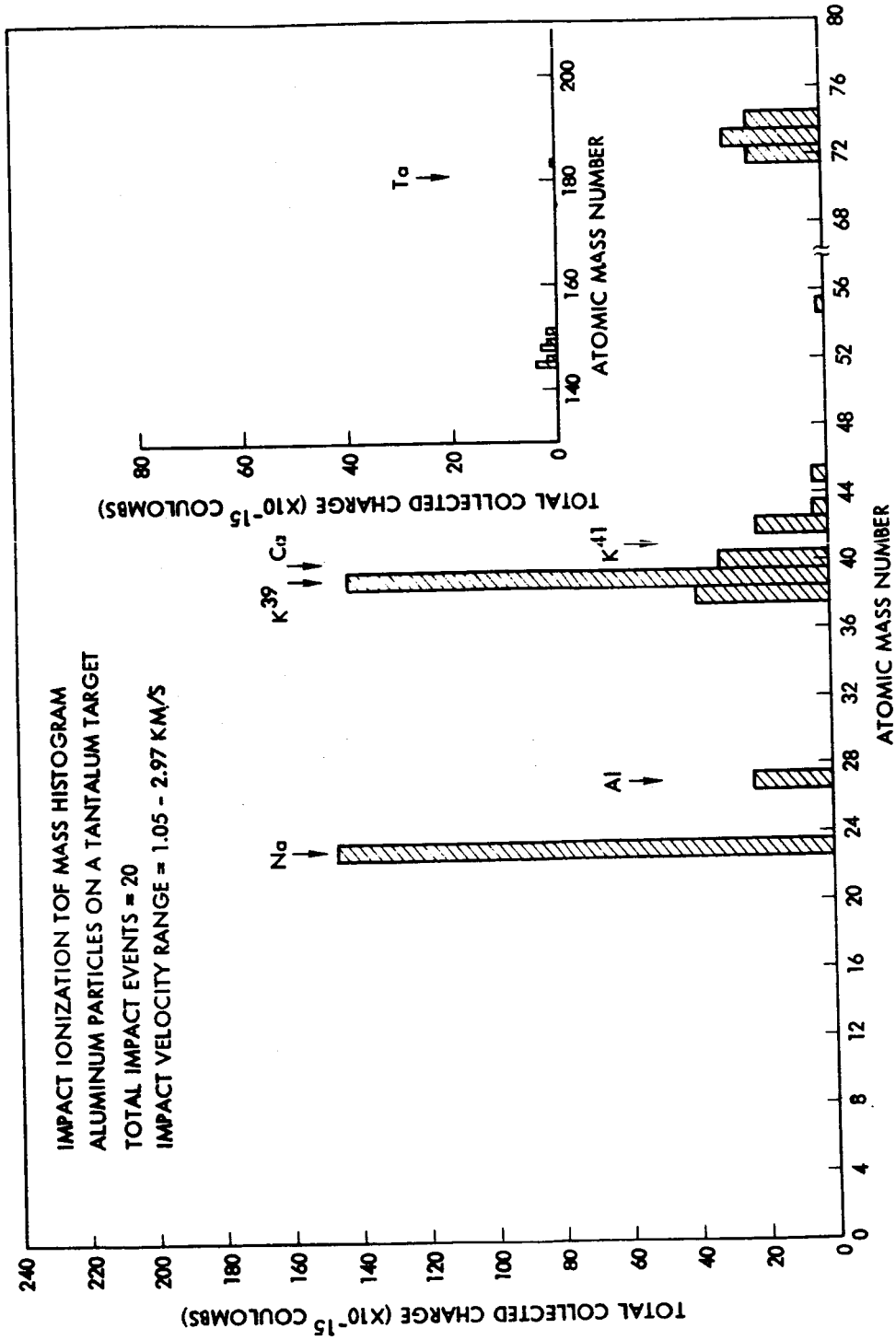

Figure 3-19. Mass Histogram of Collected Charge for Aluminum Particles on a Ta Target, using ion TOF. Particle impact velocity range is 1.05 - 2.97 km/s.

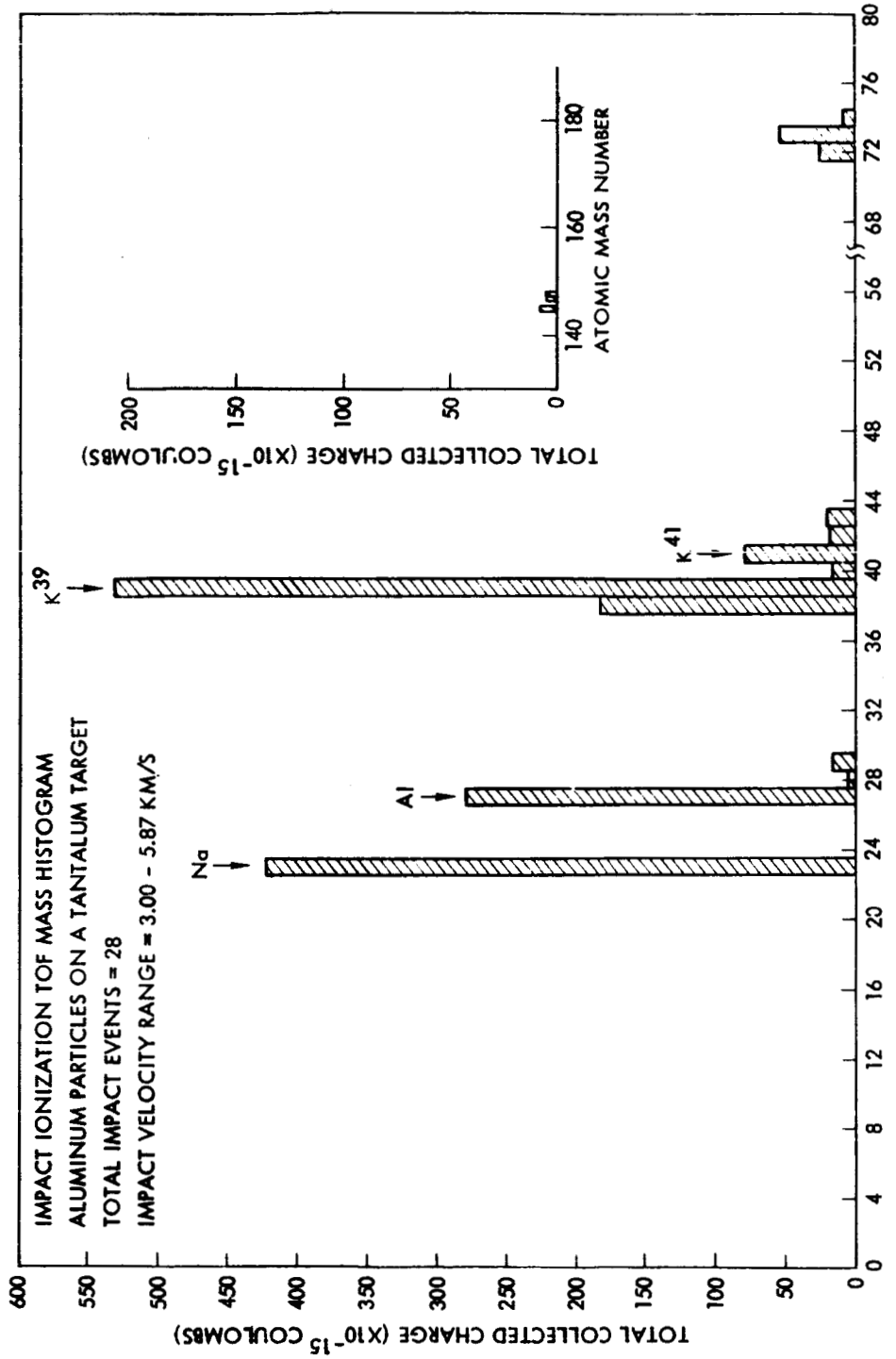

Figure 3-20. Mass Histogram of Collected Charge for Aluminum Particles on a Ta Target, using ion TOF. Particle impact velocity range is 3.00 - 5.87 km/s.

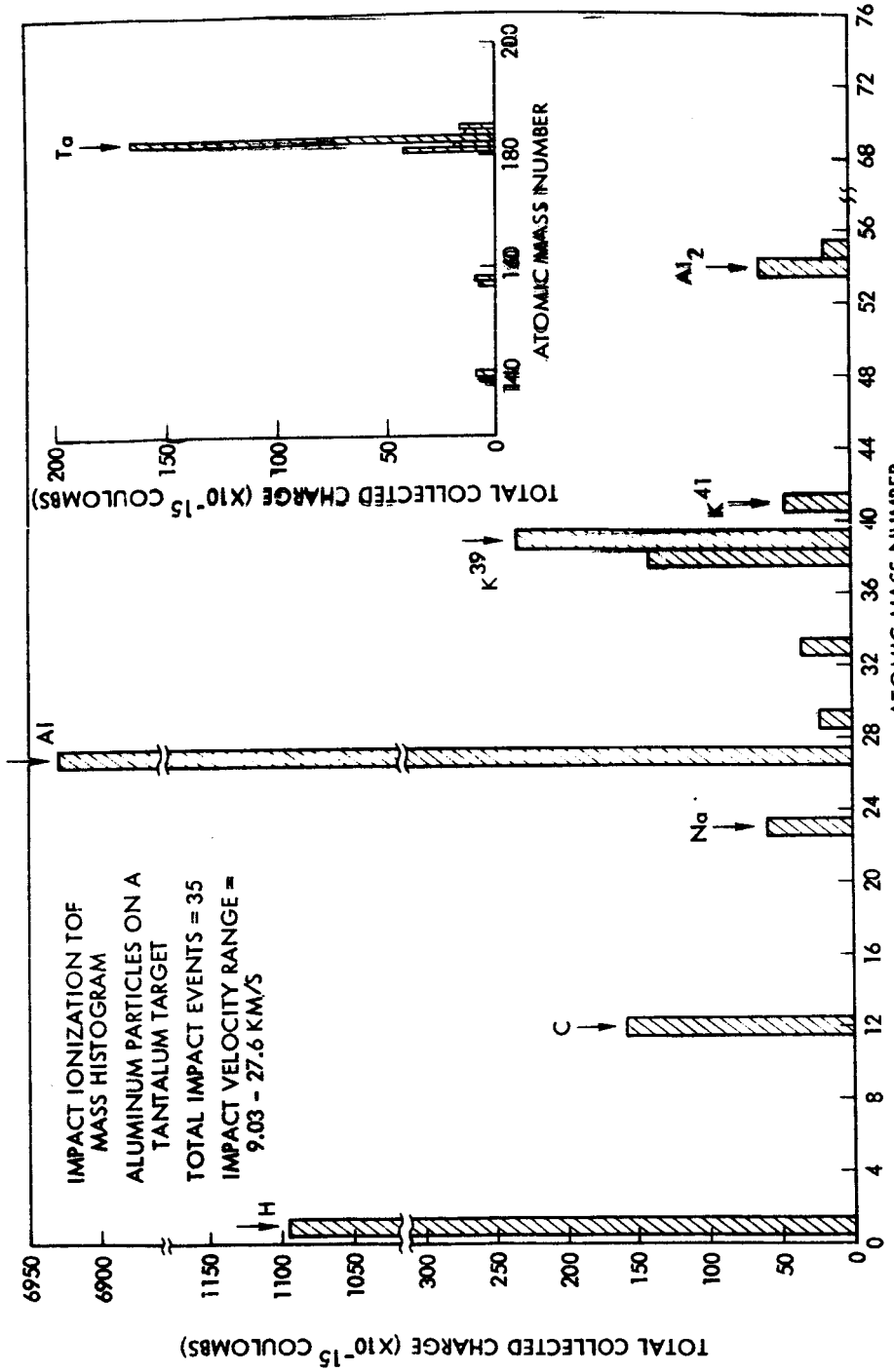

Figure 3-21. Mass histogram of Collected Charge for Aluminum Particles on a Ta Target, using ion TOF. Particle impact velocity range is 6.02 - 8.97 km/s.

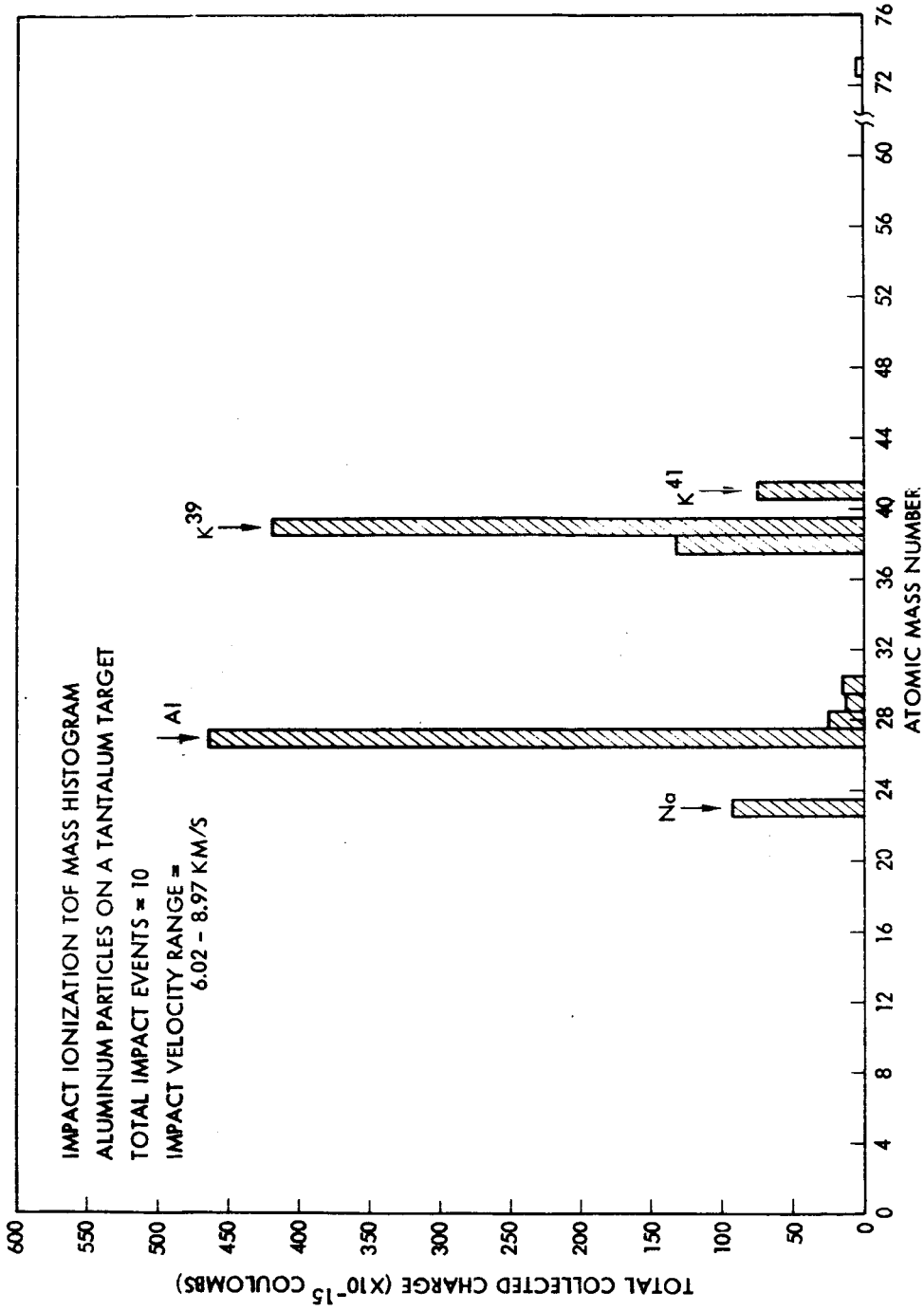

Figure 3-22. Mass Histogram of Collected Charge for Aluminum Particles on a Ta Target, using ion TOF. Particle impact velocity range is 9.03 - 27.6 km/s.

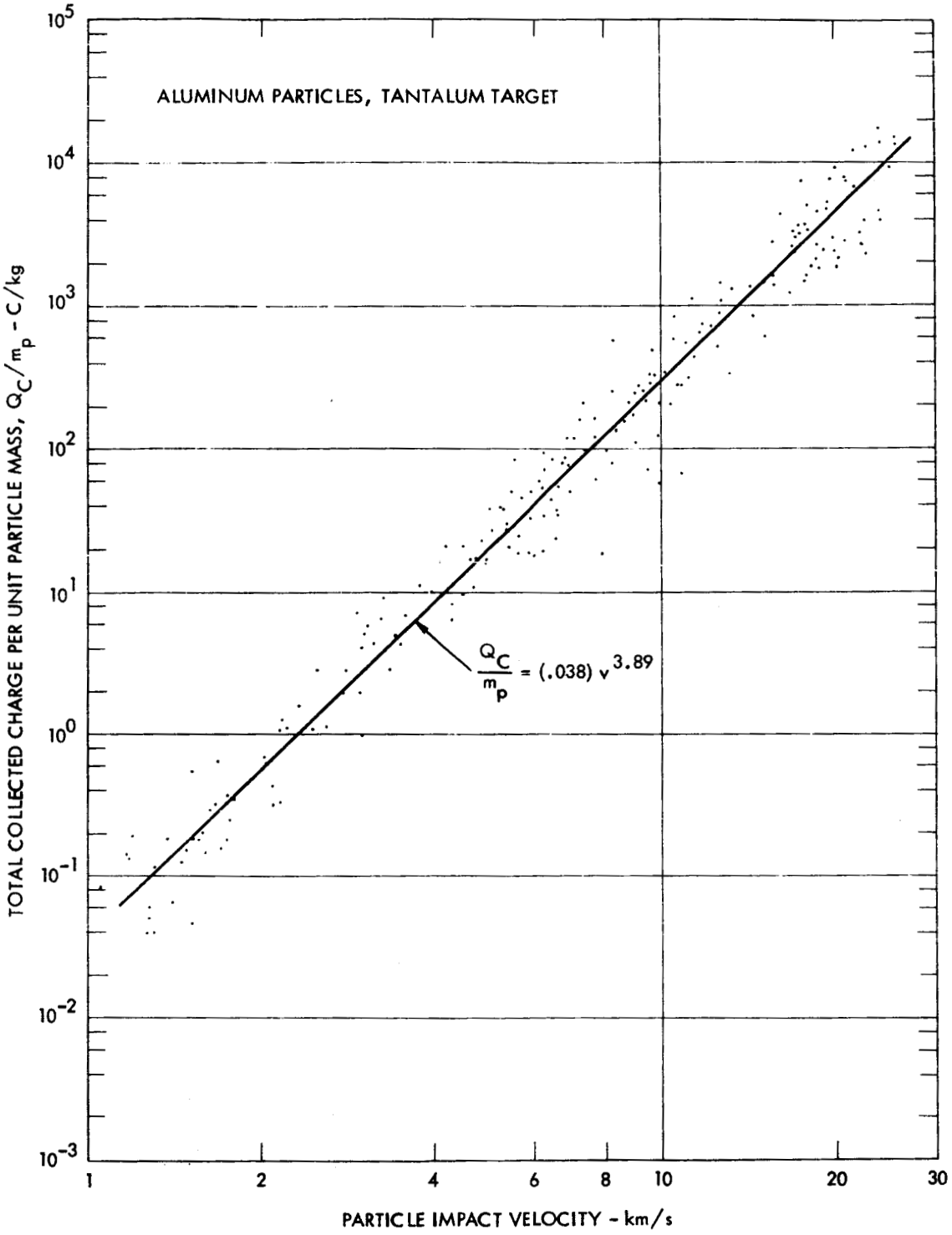

Figure 3-23. Total Collected Charge Per Unit Particle Mass Q_c/m_p vs Particle Impact Velocity: Aluminum Particles, Ta Target.

in such large relative quantities is immediately questioned since the target and particle materials are known to be low in impurities. However, the large relative difference in degree of ionization between sodium and potassium and the higher ionization potential materials is not inconsistent with the plasma model. It simply means that the "equilibrium" temperature of the impact plasma is low and apparently drops with decreasing impact velocity. As was described in Section 2.0, the ionization potential is probably the most important parameter for production of impact ionization. The relative signal sensitivity to this parameter will now be considered.

The above effect may be illustrated by an examination of the expected ion ratio of two materials contained in a plasma in thermal equilibrium. By taking the ratio of the Saha equation (from Section 2) for thermal ionization of one material to that of a second material, the following equation may be written:

$$\frac{N_i^{(1)}}{N_i^{(2)}} = \frac{N_n^{(1)}\, P^{(1)}}{N_n^{(2)}\, P^{(2)}} \exp\left[\frac{E_I^{(1)} - E_I^{(2)}}{KT}\right] .$$

In the above, N_i is the ion number density of the respective materials and N_n is the neutral number density in the plasma. $P^{(1)}$ and $P^{(2)}$ are the partition functions of materials (1) and (2) respectively and are generally a function of temperature. E_I is the energy required for ionization of the respective element, K is the Boltzmann's constant, and T is the plasma temperature in degrees Kelvin.

The above equation was used to compute the expected ion ratios for several materials with two simplifying assumptions: (1), the ratio of the neutral number density is unity; (2), the ratio of the partition functions is equal to unity across the range of calculated temperatures. The results obtained are shown in Figure 3-24 where the expected ion ratio has been plotted against the plasma temperature.

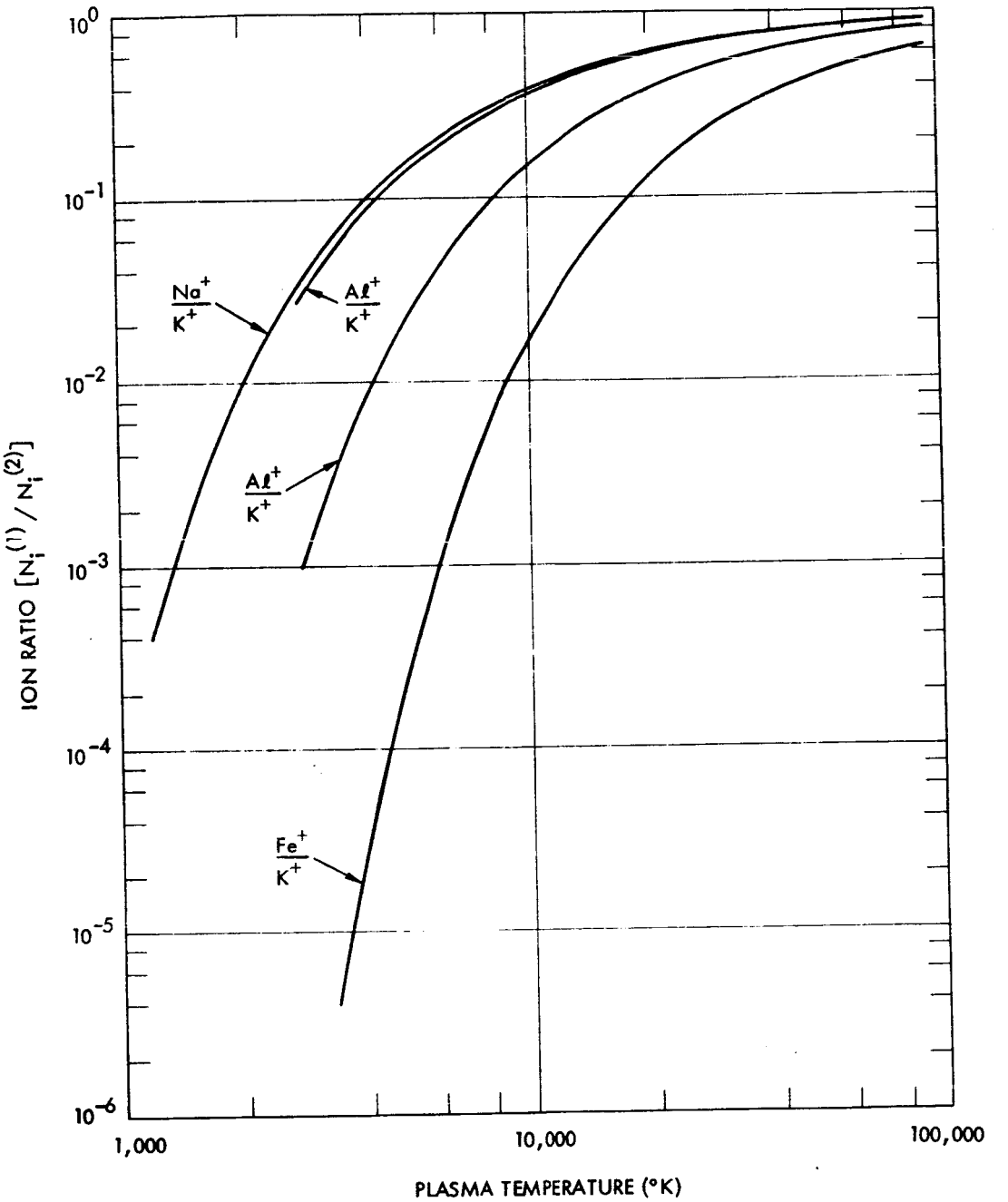

Figure 3-24. Computed Ion Ratio vs Plasma Temperature. In each case, the minimum temperature plotted is the maximum of the two vaporization temperatures of the elements forming the ratio.

The expected ion ratios are shown for Na^+/K^+, $A\ell^+/Na^+$, $A\ell^+/K^+$, and Fe^+/K^+. The ionization potential for these elements are 5.138 eV for sodium, 4.339 eV for potassium, 5.998 eV for aluminum, and 7.87 eV for iron. The curves sketched show the expected ratio from the vaporization temperature of the highest temperature element of the pair up to 100,000°K. It may be seen that for very low temperatures extremely small ion ratios are to be expected. For example, at the vaporization temperature of iron, the ratio of Fe^+/K^+, for equal neutral number density in the plasma is on the order of 1×10^{-5}. Another way of stating this is that with 0.1% potassium in an iron-potassium mixture the expected number of K^+ per unit volume will be 100 times larger than the number density of Fe^+.

The plasma model therefore predicts high signal levels of low ionization potential materials if the temperature is low. It is reasonable to assume that the plasma temperature does decrease as particle impact velocity decreases.

3.4 Impacts on Thin Film Semiconductor Detector

It is clear from the foregoing discussion that the dependence of impact ionization on ionization potential of the elements involved complicates the use of the phenomena in a device to perform composition analysis. It has been suggested that a means for avoiding this complication is to use a thin film capacitor which has one electrode sufficiently thin to be penetrated by an impacting particle. If the particle penetrates at least part way through the dielectric material then an electrical discharge may be induced at the point of impact. When simply phrased, the suggestion is that the electrical current through the impact crater region would serve to fully ionize the impacting particle material.

In order to explore this concept, a thin film capacitor type detector was used which consisted of a 5.1 cm diameter P-type silicon substrate with a 4000 Å silicon dioxide layer as a dielectric. The second plate of the capacitor was a 1500 Å vacuum deposited aluminum film. Impact tests were conducted in the TOF chamber using carbonyl iron particles. The impact surface of the detector was mounted 1.0 cm behind the target grid plane. Capacitor bias was 50 volts.

Initially, the detector was treated as a standard target and biased 3000 volts positive with respect to the grounded target grid. Particle impacts at 5 km/sec caused excessively large signals on the target output lead which appeared to be due to voltage breakdown of the target. Collector signals were received which were large amplitude slow rising pulses with no distinquishable steps from which mass groups could be identified. The large signals continued as the bias voltage was reduced down to 150 volts target bias at which point one could tell that an impact caused a large quantity of charge to leave the target without causing voltage breakdown. No ion groups were resolved on the collector signal.

A 1.0 microfarad capacitor was placed from target to ground to reduce the amplitude of the target signals to prevent possible "smearing" of ion energies as the potential changed. The unit operated consistently without breakdown at 150 volts; however, the collector signal at no time showed any resolveable mass groups.

The conclusion from the test is that this type of unit will not function adequately in an impact TOF mass analyzer. In the tests performed, charge was seen to be emitted from the target gas for more than 50 microseconds which would serve to degrade the system time resolution to unacceptable levels. A second detrimental feature is the quantity of charge produced. It is so excessively large that extreme difficulty would be found in rejecting the undesired charge, especially since even minute quantities of impurities could mask the desired elements from the particle material.

4.0 SUMMARY AND DISCUSSION

Three possible approaches to the in situ measurement of chemical composition of cometary or asteroidal particles have been identified: (1) One technique would be to utilize a collection type instrument that would perform a chemical analysis on a particle or number of particles acquired more or less intact. It would seriously strain the present state of the art to produce such an instrument capable of analyzing a single micron size range particle on any reasonable sized collector. However, it seems feasible to envision an instrument that would perform such an analysis on a relatively large number of particles as might be obtained by a comet intercept mission. A measure of the average composition of all particles could conceivably be obtained in this fashion. No knowledge of such an instrument is presently available; however, and it would undoubtedly involve a considerable fiscal expenditure as well as a considerable period of time to develop such a device for a spacecraft mission.; (2) A second technique which has been the subject of substantial effort is that of utilizing the impact light flash. At the moment of impact of a hypervelocity microparticle, a light flash is observed that is known to be at least partially composed of line radiation. There exists the possibility of using the observed line radiation to determine the elements present in the impacting particle. Several investigators have explored this area both theoretically and experimentally with only limited success in identifying materials in the impacting particle.[12,13,14] The development of this technique is still in the rudimentary stages and appears to be a highly complex approach to the identification of microparticle constituents.; (3) The third method involves the use of the impact ionization phenomena for the identification of the constituent materials in a microparticle. It is the subject of this study and at present is believed to be by far the most attractive and thoroughly developed approach to in situ measurement of chemical composition.

The impact ionization data acquired on this program show that low velocity impacts generally tend to produce measureable signals only for those elements with low ionization potentials. From these data then it is concluded that an impact ionization TOF mass analyzer could be utilized for the detection of the alkali elements down to perhaps one km/s. In

this group would fall any element or compound with ionization potential below about 5.5 eV. For detection of elements with 8 eV or greater, the impact velocity should exceed 10 km/s to obtain signal amplitudes that can be measured reliably.

For a possible comet intercept mission in the 1-8 km/s range, an impact ionization TOF mass analyzer could achieve limited success in the detection and characterization of impacting particles. However, recommendations are that higher velocity intercept missions be considered for this instrument since the data yield increases so markedly with increasing velocity. It would be especially advantageous to use higher velocity impacts since the apparent higher plasma temperature will permit the observation of control elements added to the target. The presence of these control elements in the output TOF signal spectrum allows a relative abundance determination to be made on those materials in the impacting microparticle which produce a measureable ion signal. The ability of the approach to yield relative abundance measurements, in addition to mass identification, has been shown in the work performed under NAS9-9309 (Reference 1) and published in Reference 15.

The recently released Final Report of the Comet Encke Ballistic Mission Engineering Panel[16] defines three possible intercept missions to Comet Encke during its 1980 apparition. The nominal intercept velocities of the three missions described are 7.3 km/s, 18 km/s, and 27 km/s. Based on the studies performed under this program and on that of Reference 1, an impact ionization time-of-flight mass analyzer could produce considerable data even on the 7.3 km/s intercept; however, the 18 km/s and 27 km/s intercepts offer substantially more data return on particle composition. The higher velocity intercept would, of course, be the more attractive of the three since it would produce larger signals from the higher ionization potential materials. The output TOF signal response would then be a more complete representation of the chemical makeup of the impacting particle.

The iron particle impacts obtained on this program from the Van de Graaff accelerator and from the linear accelerator indicate that impact ionization is strongly dependent on particle mass. It is assumed that the equation for the impact charge produced may be expressed as

$$Q = K m_p^{\alpha} v^{\beta}$$

where, K = a materials constant,

m_p = particle mass,

v = particle velocity.

The data presented herein show that the value of α at 10.0 km/s with a tantalum target is 0.154. This value differs substantially from what other investigators have found. Auer and Sitte[17] (1968) found that $\alpha = 1.0$ at $v = 2.8$ km/s, and $\alpha = 0.7$ at $v = 5.9$ km/s for iron particles on a tungsten target. Dietzel, Neukum, and Rauser[18] (1972) found for a tungsten target that $\alpha = 1.0$ for $v < 2$ km/s, and $\alpha = 0.9$ for $2 < v < 9$ km/s. Smith and Adams[19] (1973) (tungsten target) found that $\alpha = 1.33$ for $v < 1$ km/s and $\alpha = 0.85$ for $v > 1$ km/s.

Although the trend is toward a lower mass exponent for these data as velocity increases, none of the reported values are as low as the one found here. It should be noted; however, that a different target material was used in each case. Also, and perhaps more importantly, the method of extracting the free charge differs markedly from that used for this study. Another noteable difference is that the average particle mass in the present data was at least an order of magnitude larger than that used by other investigators near 10 km/s.

REFERENCES

1. Friichtenicht, J.F.; Roy, N.L.; and Moede, L.W.: Cosmic Dust Analyzer. TRW Systems Group Report 10735-6002-RO-00 (Contract NAS9-9309, Final Report), March, 1971.

2. Friichtenicht, J.F.; Slattery, J.C.: Ionization Associated with Hypervelocity Impact. NASA TN D-2091, 1963.

3. Independent Research and Development Program Annual Progress Report, Section XI, Space Sciences, TRW System Group Document 9990-7297, 1965.

4. Hanson, D.O.: Mass Analysis of Ions Produced by Hypervelocity Impact. Appl. Phys. Letters, Vol. 13, No. 3, pp. 89-91, August, 1968.

5. Bjork, R.J.: Review of Physical Processes in Hypervelocity Impact and Penetration. Proceedings of the Sixth Symposium on Hypervelocity Impact, Vol. II, Part I, published by the Firestone Tire and Rubber Company, August, 1963.

6. Sutton, G.W.; and Sherman, A.: Engineering Magnetohydrodynamics. McGraw-Hill Book Co., New York, 1965.

7. Friichtenicht, J.F.: Two-Million-Volt Electrostatic Accelerator for Hypervelocity Research. Rev. of Sci. Instr., Vol. 33, No. 2, pp. 209-212, February, 1962.

8. Shelton, H.; Hendricks, C.D.; and Wuerker, R.F.: Electrostatic Acceleration of Microparticles to Hypervelocities. Journ. of Appl. Phys., Vol. 31, No. 7, pp. 1243-1246, July, 1960.

9. Roy, N.L.; and Becker, D.G.: A Time Interval Selector and Proportional Delay Generator. Rev. of Sci. Instr., Vol. 42, No. 2, pp. 204-209, February, 1971.

10. Hansen, D.O.; and Roy, N.L.: A Solid-State Low-Noise Preamplifier. Nuclear Instruments and Methods, Vol. 40, pp. 209-212, North-Holland Publishing Company, Amsterdam, 1966.

11. Slattery, J.C.; Becker, D.G.; Hamermesh, B.; and Roy, N.L.: A Linear Accelerator for Simulated Micrometeors. Rev. of Sci. Instr., Vol. 44, No. 6, pp. 755-762, June, 1973.

12. Harwell, Kenneth E.; Reid, James L.; and Hughes, Albert R.: Calculated Equilibrium Composition and Radiation of Metallic Plasmas Produced in Hypervelocity Impact. Journal of Spacecraft, Vol. 8, No. 4, pp. 358-366, April, 1971.

13. Jean, B.; and Rollins, T.L.: Radiation from Hypervelocity Impact Generated Plasma. AIAA Journal, Vol. 8, No. 10, pp. 1742-1748, October, 1970.

14. Jean, B.; and Alexander, K.: Meteoroid Impact Flash Analyzer, Final Report. NASA CR-115066 (NASA Contract NAS9-8788), Report by Computing Devices of Canada Limited, Subsidiary of Control Data, 17 May, 1971.

15. Friichtenicht, J.F.; Roy, N.L.; and Becker, D.G.: The Cosmic Dust Analyzer: Experimental Evaluation of an Impact Ionization Model. Evolutionary and Physical Properties of Meteoroids, NASA SP-319, (Proceedings of the International Astronomical Unions Colloguium #13, held at State University of New York on June 14-17, 1971), 1973.

16. Ballistic Intercept Missions to Comet Encke: Final Report of the Comet Encke Ballistic Mission Engineering Panel. NASA Technical Memorandum, NASA TM X-72542, March, 1975.

17. Auer, S.; and Sitte, K.: Detection Technique for Micrometeoroids Using Impact Ionization. Earth and Planetary Science Letters, Vol. 4, No. 2, pp. 178-183, April, 1968.

18. Dietzel, H.; Neukum, G.; and Rauser, P.: Micrometeoroid Simulation Studies on Metal Targets. Journ. of Geophys. Res., Vol. 77, No. 8, pp. 1375-1395, March 10, 1972.

19. Smith, D.; and Adams, N.G.: Studies of Plasma Production at Hypervelocity Microparticle Impact. Journ. of Physics D: Appl. Phys., Vol. 6, pp. 700-719, 1973.